ISTANBUL TECHNICAL UNIVERSITY ★ INSTITUTE OF SCIENCE AND TECHNOLOGY

COMPUTATIONAL ANALYSIS OF EXTERNAL STORE CARRIAGE IN TRANSONIC SPEED REGIME

M.Sc. Thesis

İ. Cenker ASLAN, B.Sc.

Department: **Aeronautical Engineering**

Programme: **National and International Integrated Graduate Program: Special Program for Turkish Airforce Personnel**

JANUARY 2003

ISTANBUL TECHNICAL UNIVERSITY ★ INSTITUTE OF SCIENCE AND TECHNOLOGY

COMPUTATIONAL ANALYSIS OF EXTERNAL STORE CARRIAGE IN TRANSONIC SPEED REGIME

M.Sc. Thesis

İ . Cenker Aslan, B.Sc.

(511011017)

Date of Submission : 24 December 2002

Date of Defence Examination : 13 January 2003

Supervisor : Assoc. Prof. Dr. Aydın MISIRLIOĞLU (İ.T.Ü.)

Co-Supervisor : Prof.Dr. Oktay BAYSAL (O.D.U.)

Members of Committee : Prof.Dr. M. Fevzi ÜNAL (İ.T.Ü.)

Assoc. Prof. Dr. F. Oğuz EDİS (İ.T.Ü.)

JANUARY 2003

İSTANBUL TEKNİK ÜNİVERSİTESİ ★ FEN BİLİMLERİ ENSTİTÜSÜ

HARİCİ YÜK TAŞIMANIN TRANSONİK SÜRAT BÖLGESİNDE HESAPLAMALI ANALİZİ

YÜKSEK LİSANS TEZİ
İ. Cenker Aslan
(511011017)

Tez Teslim Tarihi : 24 Aralık 2002

Tez Savunma Tarihi : 13 Ocak 2003

Tez Danışmanı : Doç. Dr. Aydın MISIRLIOĞLU (İ.T.Ü.)

Eş-Danışman: Prof.Dr. Oktay BAYSAL (O.D.U.)

Jüri Üyeleri : Prof.Dr. M. Fevzi ÜNAL (İ.T.Ü.)

Doç. Dr. F. Oğuz EDİS (İ.T.Ü.)

OCAK 2003

ACKNOWLEDGMENTS

I would like to express my sincere appreciation to my advisors, Dr. Oktay Baysal, ODU, and Dr. Aydın Mısırlıoğlu, ITU, for their valuable guidance and support during the entire course of this study. I also would like to express my gratitude to my committee members for their useful comments and suggestions during my thesis preparation.

Special thanks are also extended to Dr. Fırat Oğuz Edis and Dr. Alim Rüstem Aslan for providing essential support in generating the computational grids. Their encouragement, assistance and friendship have also been of immense help in finishing this research. The moral and technical support of research assistants, department secretaries and my Air Force colleagues is also appreciated.

I would like to express my sincere respect for Turkish Air Force for funding this entire program.

Finally, I would like to take this opportunity to express my deepest love, appreciation and gratitude to my wife for her continuous support and encouragement.

Thank you very much.

Cenker ASLAN
December 2002

CONTENTS

LIST OF TABLES

Biçimlendirilmiş: Sol: 4,01 cm

LIST OF FIGURES

Biçimlendirilmiş: Yazı tipi: 12 nk

Biçimlendirilmiş: Sola

Biçimlendirilmiş: Sola, Girinti: Sol: 0 cm, İlk satır: 0 cm, Aralık Önce: 71 nk, Sonra: 18 nk, Satır aralığı: tek, Sekme durakları: Eskisi 8,62 cm

LIST OF SYMBOLS

a	: speed of sound
$\tilde{A}$	: Roe-Averaged Flux Jacobean Matrix
A_{ij}	: cell face area
AOA	: angle of attack
C_N	: normal force coefficient
C_D	: drag coefficient
C_L	: lift coefficient
C_p	: pressure coefficient
CFD	: computational fluid dynamics
CFL	: Courant-Friedrichs-Lewy number
CFL3D	: Computational Fluids Laboratory 3-Dimensional flow solver
CPU	: central processing unit
d	: diameter
DDT	: Domain Decomposition Technique
e	: total energy
e_0	: energy per unit volume
$\vec{E}$	: inviscid flux vector
FD	: Finite Difference
FDS	: Flux Difference Splitting
FV	: Finite Volume
FVS	: Flux Vector Splitting
$\vec{F},\vec{G},\vec{H}$	: flux vectors in cartesian coordinates
$\hat{F},\hat{G},\hat{H}$	: flux vectors in curvilinear coordinates
h	: enthalpy
h_0	: enthalpy per unit volume
J	: transformation Jacobean
k	: cell face
M_∞	: free stream mach number
MaGGiE	: Multi Geometry Grid Embedder
n	: unit normal
$\hat{n}$	: outward facing unit normal
$\vec{N}$	: outward pointing normal to the boundary
OCO	: ogive cylinder ogive

ONC	: ogive nose cylinder
p	: pressure
P	: static pressure
Q	: conserved variables
$\vec{Q}$	: conserved variables in vector form
$\hat{Q}$	: conserved variables in curvilinear coordinates
Q_L	: conserved variables to the left of the interface
Q_R	: conserved variables to the right of the interface
R_i	: residual
$R^{\pm}$	: Riemann invariants
t	: time
T	: temperature
u, v, w	: velocities in cartesian coordinates
U, V, W	: contravariant velocities
$\vec{V}$	: velocity vector
V_i	: volume
x, y, z	: cartesian coordinates of grids
α	: angle of attack in degree
$\tilde{\Gamma}$	: right eigenvectors of Roe-averaged flux Jacobean matrix
$\tilde{\Gamma}^{-1}$	: left eigenvectors of Roe-averaged flux Jacobean matrix
γ	: ratio of specific heats
ρ	: density
ξ, η, ζ	: generalized curvilinear coordinates
$\Delta_{\pm}$	: forward and backward differencing
Λ	: diagonal matrix
Δ	: change

University	**:**	**Istanbul Technical University**
Institute	**:**	**Institute of Science and Technology**
Science Programme	**:**	**Aeronautical Engineering**
Programme	**:**	**Aeronautical Engineering**
Supervisor	**:**	**Assoc. Prof. Dr. Aydın MISIRLIOĞLU**
Degree Awarded and Date	**:**	**Ms – January 2003**

ABSTRACT

COMPUTATIONAL ANALYSIS OF EXTERNAL STORE CARRIAGE IN TRANSONIC SPEED REGIME

Cenker ASLAN

In the present work, a computational application and analysis of external store carriage is studied in a transonic speed region. Computational Fluid Dynamics (CFD) is used as a methodology in order to analyze this phenomenon. The interference flowfield between NACA64A010 airfoil and Ogive Cylinder Ogive (OCO) combination at various angles of attack and different external store locations is investigated at 0.95 Mach. A composite grid generator, MaGGiE, which uses grid overlapping method of domain decomposition technique, is used to create the two dimensional composite grid for the complex geometry. A new version of CFL3D, a finite volume solver for the structured grids, is used as the flow solver. In this study, Inviscid Euler equations are solved by implementing a steady state, implicit, approximately factored, upwind biased method in order to investigate interference flowfield of this complex geometry. The demonstration of the results is accomplished by plotting contour lines and Cp plots of the cases. The results are compared with the results in the literature, and they are in good agreement.

Keywords: CFD, External Store, Composite Grids, Transonic Speed.

Science Code: 618

Üniversitesi	**: İstanbul Teknik Üniversitesi**
Enstitüsü	**: Fen Bilimleri**
Anabilim Dalı	**: Uçak Mühendisliği**
Programı	**: Uçak Mühendisliği**
Tez Danışmanı	**: Doç. Dr. Aydın MISIRLIOĞLU**
Tez Türü ve Tarihi	**: Yüksek Lisans – Ocak 2003**

ÖZET

HARİCİ YÜK TAŞIMANIN TRANSONİK SÜRAT BÖLGESİNDE HESAPLAMALI ANALİZİ

Cenker ASLAN

Bu çalışmada, transonik sürat bölgesinde harici yük taşımanın hesaplamalı analizi ve uygulaması yapılmıştır. Bu problemin analizinde metod olarak hesaplamalı akışkanlar dinamiği (CFD) kullanılmıştır. NACA64A010 kanadı ile ön ve arka kısmı "ogive" şeklindeki bir silindirin (OCO) bu kanadın altına yerleştirilmesi ile elde edilen kompleks geometrinin birbirleriyle etkileşimli akış alanları farklı hücum açıları ve farklı harici yük pozisyonlarında hesaplanmıştır. Bu kompleks geometriye ait iki boyutlu kompozit grid, "grid overlapping" metodunu kullanan MaGGiE adlı bir kod kullanılarak hazırlanmıştır. Tüm problemler CFL3D adı verilen ve "finite volume" metodu kullanan bir çözüm algoritması kullanılarak hesaplanmıştır. Çözümlerde zamana bağımlı olmayan "Inviscid Euler" denklemleri kullanılmıştır. Geometrilerin birbirlerinin akış alanını etkilediği karmaşık bölgelere ait kontur çizgileri ile basınç katsayılarındaki değişim çizimlerle gösterilmiştir. Elde edilen sonuçlar literatürdeki sonuçlarla karşılaştırılmış ve birbirleri ile oldukça uyumlu oldukları görülmüştür.

Anahtar Kelimeler: CFD, Harici Yük, Kompozit Grid, Transonik Sürat.

Bilim Dalı Sayısal Kodu: 618

1. INTRODUCTION

1.1 Motivation

It is ~~very well~~commonly known that the primary missions of military fighter aircraft ~~is~~are to carry and launch air-to-air missiles or to release ~~the~~ air-to-ground attack weapons to a~~the~~ target. In addition~~Besides~~, aircraft usually must~~have to~~ carry external fuel tanks to increase their range of flight. Carriage of these kinds of stores becomes an important handicap to increase aircraft speed, maneuverability for performance and decrease ~~its~~ radar cross-section to enhance survivability. One method of accomplishing these goals is to mount the stores closer to the aircraft surface like tangential or semisubmerged carriage, instead of pylon, ~~carriage~~ or to carry the stores inside the aircraft. Each of these methods has some advantages or disadvantages that must be considered during the aircraft design process.

Historically, aircraft have usually carried stores on pylons mounted below the wing and fuselage. Although aircraft were developed to be aerodynamically clean, the roles of many aircraft have changed throughout their operational lives~~fe~~ as new versions ~~of the aircraft~~ were developed, necessitating the carriage of wide variety of weapons such as air-to-air missiles, ground attack weapons and ~~or~~ stores like external fuel tanks. Wing-pylon-store carriage provided a relatively easy method for meeting the variety carriage configurations required for these aircraft. Although low drag wing pylon carriage configurations have always been important to ~~the~~ aircraft designers, wing pylon mounts have proven to have unacceptable drag penalties at supersonic speeds.

Problems related to store carriage and separation will continue to be important since existing aircraft originally designed for external carriage will remain in service for a long time. Moreover, as new stores are put in service or investigations of aircraft and new store compatibility can be the other problems ~~about~~ in store carriage and

Biçimlendirilmiş: Yazı tipi: 12 nk
Biçimlendirilmiş: Sola, Satır aralığı: 1,5 satır
Biçimlendirilmiş: Girinti: İlk satır: 0 cm, Aralık Önce: 18 nk, Sonra: 12 nk
Değiştirilmiş Alan Kodu
Biçimlendirilmiş: Yazı tipi: 12 nk, Kalın
Biçimlendirilmiş: Normal, İki Yana Yasla, Girinti: Sol: 0 cm, Hecele
Biçimlendirilmiş: Girinti: İlk satır: 0 cm

separation. One of the most important problems associated with store carriage is the safe separation of stores from a pylon or weapon bays of aircraft. The release of stores from maneuvering aircraft with additional chances of physical interference also remains important.

The problem of separating a store from an aircraft has plagued aircraft and weapons designers since the aircraft was first used to deliver stores. Interference effects between the store and aircraft can often perturb the trajectory of the store to such an extent that it cannot hit the desired target area. The complexity of this problem has increased with the increase in the aircraft speed. The magnitude of the interference forces at high speeds has become so large that in some cases designers have to be concerned not only with hitting the target but also with a safe separation of the store from the aircraft. These large interference effects are particularly prevalent for stores separating from a wing pylon or cavities, specifically from shallow cavities.

The most complex flow that is encountered in a store carriage and separation scenario may be the one in which the airplane/store is in transonic speed regime. In such a speed regime, shock waves will exist and interact. In addition, the airflow may separate due to angle of attack effects or shock/boundary layer interaction. ~~Shortly, t~~These interference flowfields in transonic speed regime are the primary concern of this thesis~~dissertation~~. Among the many other methods to analyze this phenomenon, Computational Fluid Dynamics is used as a method in this study.

Computational Fluid Dynamics (CFD) ~~, shortly called CFD,~~ plays a dominant role in the aerospace field because of the realization that CFD is an effective design tool that~~, which~~ complements and goes beyond experimental tests. In addition, ~~Besides,~~ CFD is relatively inexpensive as ~~it is~~ compared with the fabrication and ~~the~~ testing of experimental wind tunnel models. However, there are costs involved, and expertise is needed to calculate flow fields over such complex geometries. Because of the rapid development of CFD in the last twenty years, efficient solvers~~,~~ capable of solving the partial differential equations of fluid flow by finite difference, finite element~~,~~ and finite volume techniques have evolved. Validations of the codes have caused the important merging of computational and experimental methods. As a result, it has become very practical to solve and analyze complex flows.

Biçimlendirilmiş: Girinti: Sol: 0 cm

1.2 Literature Survey

With continuing advances in CFD methods and improvements in calculation speed and storage capacity using modern and large scale computers, the need for experimental data to solve store carriage and separation problems would seem to be lessening. However, there is no single method that has been verified for a complete range of aircraft/store combinations or flow conditions. Store carriage and separation at transonic speeds, multiple carriage~~,~~ and separation from multiple carriage configurations have been and continue to be extremely difficult to handle analytically. In the future, new aircraft/store configurations, super maneuvering aircraft, unconventional store shapes and store separation at hypersonic speeds will offer new challenges. Assessment of safe and optimum store release for each of these areas will probably require some experimental testing. Additionally, development and verification of prediction methods~~, including CFD~~ applicable to these problem areas, including CFD, always require experimental data.

Experimental techniques for examining store separation in the wind tunnel are well developed [1, 2]. These types of wind tunnel tests can be expensive and therefore cannot cover the complete range of geometrical, flow and launch conditions. For example, Schlieren photographs are not always available and vapor screen photographs are limited in providing information. The effects of maneuvering aircraft on the aerodynamic loads and on the trajectory of a launched store are difficult to simulate in the wind tunnel. In addition, wind tunnel models of aircraft are usually solid, stiff, and do not deform in the same manner as full-scale aircraft. However, certain wind tunnel tests are always necessary to establish grid databases and to verify prediction methods, especially in the transonic speed regime. There are certain wind tunnel testing techniques for store carriage and separation: ~~, which are~~ Captive Trajectory System, Free Drop~~,~~ and Grid Survey& Flow Angularity Data Bases [3].

Accepted as another technique, ~~F~~flight-testing ~~accepted as another technique,~~ involving separation of new stores is universally regarded as expensive and dangerous for ~~the~~ flight safety. In addition to hardware~~—~~related tests of store compatibility in carriage, flight tests are often conducted to validate and verify

Biçimlendirilmiş: Yazı tipi: 12 nk

Biçimlendirilmiş: Girinti: İlk satır: 0 cm

preflight prediction analysis and to check and complement wind tunnel tests. Flight tests are especially useful for store carriage and separation studies in transonic speed regime, for ripple or continuous release of stores from several carriage locations and for cases involving carriage and launch from a maneuvering aircraft. The latter problemsuseones are especially difficult to simulate in wind tunnel testing.

As a methodology, store separation data from flight tests are usually recorded with a camera. Nevertheless, the number of complete television pictures per unit time in these records may be too low for adequate analysis of the store separation trajectories. The other technique is to place cameras on a chase plane. In any event, data reduction methodologies are required to translate the recorded motion to displacements and angular positions as a function of time. Some detailed descriptions of recorded data postprocessors are given in reference [2]. Besides, tThe engineers who investigate store carriage and separation phenomenon must use their best judgment based on experience and the availability of more than one set of data and or prediction methods. As a result, for the store carriage and separation problems, the agreement among flight tests, wind tunnel tests, and prediction methods has tomust be confirmed and approved.

Rapid advances in computer hardware and architecture have made it possible to solve complex flow problems using computational fluid dynamics. that is commonly known as CFD. The objective of CFD is to solve the system of partial differential equations, which govern the fluid flow using discrete methods. An essential element of a CFD solutions is the construction of a grid or, in other words, mesh on which the flow equations are solved in a finite form. A major limitation in CFD is the generation of suitable a grid for the three-dimensional complex configurations. Configurations, such as a wing and a fuselage, a wing and a store, and a wing and a nacelle are recognized as complex configurations. These configurations may consist of multiple bodies with nonsmooth, joint or disjoint components. A suitable grid has tomust accurately represent the boundaries of the configuration and conform to the expected flow conditions. Consequently, constructing a single grid about a complex configuration is either a difficult task or it may result in a skewed grid, which in turn results in an erroneous solution. Other difficulties may also arise when clustering the grid for the regions where the flow variables and their gradients change rapidly. Several different approaches have been used by researchers to reduce this

complexity and ease the grid generation efforts. They include unstructured grids, grid adaptation, and domain decomposition techniques.

Unstructured grids discretize the flow domain by arbitrary, but generally triangular or quadrilateral elements. The nodes are placed at the vertices of the elements. An unstructured grid possesses more flexibility in constructing meshes for complicated regions of the flowfield than does a structured grid. However, it requires more computer time and storage, as well as increased efforts in handling the data structure.

In grid adaptive schemes, a dynamically adaptive grid continually adjusts the flow and follows the developing gradients in the physical solution. Grid adaptation reduces the errors associated with inadequate resolution at regions of high flow gradients and oscillations, such as shocks and boundary layers. This technique combined with the domain decomposition techniques may prove to be an important tool in solving complex flow problems.

Domain decomposition technique, which is commonly known as DDT, subdivides the flow domain into simpler subdomains, which accept easily constructed grids with appropriate grid refinement. Nonsimilar grid topologies, generally independent of each other, can be generated and used to improve grid deficiencies. DDT allows employment of different solution methods for different subdomains. For example, the physical domain can be divided into two subdomains as nearfield and farfield. Various approaches exist in subdividing the flow domain and establishing the communication among these subdomains.

There are three basic types of domain decomposition techniques [4]: . These are multiblock, zonal, or patched methods and overlapped methods. It can be called as aA fourth method, the degenerate zonal method, can be derived to have partially the features of the multiblock and partially those of zonal methods.

The multiblock grid method allows any number of blocks to be employed to fill an arbitrary three-dimensional region. Any block can be linked to another block or blocks subject to constraint that the grid lines are contiguous between blocks, with one-to-one continuity in the grid lines. The union of these blocks fills the entire flowfield without holes or overlaps.

The zonal method, also known as grid patching, requires the domain to be divided into subdomains with simple and easily generated grids. These grids are then patched

together along common boundaries or surfaces to create a global grid. The grid lines in adjacent grids are not aligned with each other at the grid surface.

The overlapping method entails dividing the flow domain into regions that overlap or share common physical and computational space. Within the overlapped region, the grids communicate through data transference by an interpolation procedure. This method allows the subdomains to be no disjoint so that one mesh may be embedded completely or partially within another. This procedure permits each subdomain to be meshed independently with no requirements of continuous grid lines across boundaries. Because each subdomain grid is independent of another, the grid generation task is greatly reduced for complicated flow regions. Each subdomain mesh can be created using different grid generation techniques suitable for that particular domain. This is especially beneficial for subdomains that require high grid densities. The grid overlapping method of DDT is used in this study in order to examine the interference flow between an airfoil and an Ogive Cylinder Ogive, which is placed under airfoil.

~~Besides~~ In addition to its advantages, there are also several drawbacks of using the grid overlapping technique. One of the most important disadvantages of this technique is that it requires an overlapped region between subdomains, which may not be always possible, as in the case of an extremely small gap between two solid surfaces. Secondly, the accuracy of boundary data transference depends on the interpolation procedure, whether it is conservative or nonconservative. Finally, the accuracy and convergence speed of the solution indirectly depend on the degree of overlapping of the grids relative to the size of the subdomains. However, with careful treatment, most of the problems can be alleviated partially or completely.

One of the early grid overlapping methods was presented by Atta [5]. He developed a finite difference method to solve the full potential equations and obtained a solution for transonic flow about a configuration with multiple components. The computational model was a two-component configuration that consisted of an airfoil embedded in rectangular boundaries. The results showed that the accuracy and the convergence speed of an implicit approximate factorization scheme depended on extend of the overlapped region and the size of each subdomain. This technique was later extended to three-dimensional flows by Atta and Vadyak [6]. This full potential, implicit, approximate factorization algorithm was applied to a wing-pylon-

nacelle configuration. Separate grids were employed for each component and the grid adaptive approach was employed to optimize each grid. Each region required a separate implementation of the algorithm with the relevant boundary conditions. The solution procedure iterated several times on a given subdomain, updated other grid boundaries contained in that subdomain and preceded to the next grid.

Steger et al. [7] developed a grid overlapping technique called "CHIMERA" grid scheme. This early study was restricted to finite difference solution of two-dimensional, linearized flows. However, the subsequent studies were extended to three-dimensional Euler [8] and thin layer Navies Stokes [9] solutions of complex flows. The scheme involved the automatic connection of multiple, overlaid grids and the use of the different solution procedures for different subdomain grids. In this technique, a major grid covers the entire flow region and minor grids are then overlaid on the major grid to solve secondary features of the configuration, such as flaps, nacelles or, stores. The minor grids are overlapped fully or partially without the restriction that grids be joined in any special way. The minor grids create holes in the major grid, which are subsequently excluded from the solution in the major grid. The information between the grids is communicated through trilinear interpolation within the overlapped region. The preliminary studies proved the CHIMERA scheme to be very flexible and successful on various configurations. However, it was shown that difficulties could arise when a shock crosses grid boundaries. The mismatch of solution in the neighborhood of the expansion preceding the shock was attributed to several factors such as the nonconservative interpolation procedure, the reflecting boundary conditions imposed at the overlap and the meager extent of the overlap near the shock [10].

Dougherty et al. [11] performed some computations, which were about two elliptic surfaces in transonic speed regime, and they simulated the prescribed paths. A two-dimensional, inviscid unsteady code was used in this preliminary study to show the feasibility of the CHIMERA scheme for a future application to the problem of aircraft/store interaction and separation. In this study, a minor grid was allowed to move with respect to the major grid. The solution showed that allowing one mesh to move with respect to another does not affect adversely the time accuracy of an unsteady solution despite strong shock interaction between the major and minor bodies. Dougherty and Kuan [12] extended this previous study to the three

dimensional analysis of an elliptic body near a flat plate. A 10% thick ellipsoid of chord length of unity was placed 15% of chord below a flat plate, both following prescribed flight paths. A steady state computation of the store and the flat plate was initially performed. After reaching the steady state convergence, the solution was used as the initial condition for the time accurate calculations. A simple downward translation and a pitch up and roll rotation were investigated.

Fox and Allee [13] conducted an experimental/computational study of a transonic aircraft with store. Flow field and aircraft surface static pressure measurements were made experimentally on three different configurations to find aerodynamic forces on a pylon-mounted store. The Euler method, using the grid overlapping methods, wasere performed to support the wind tunnel measurements. Both experimental and computational tests concluded that the dominant effect on the store is the gross sideways of the vehicle distributed along the length of the store, causing yaw forces in the direction that would move the nose of the store away from the centerline of the fuselage. In addition, this study proved that a solution of the Euler equations over such a complex configuration has become practical, both for pretest prediction and for posttest analysis.

Meakin and Suhs [14] developed a prototype method for time accurate simulation of multiple aerodynamic bodies in relative motion. This method featured the unsteady CHIMERA domain decomposition technique and an implicit, approximately factored, finite difference procedure to solve the time dependent thin-layer Navier-Stokes equations. Several steady and unsteady configurations were considered as test cases and two configurations were used to demonstrate the prototype method. First, a body was released from its position placed under a wing. Then, the separation of an integrated space shuttle from its solid rocket booster was considered. The converged steady state solutions for both configurations were obtained. Then, these steady state results were used as the initial conditions for the unsteady store separation problems. In both cases, the released objects were moved in prescribed paths.

Chow and Marconi [15] obtained a three dimensional Navier Stokes solution of hypersonic flow past a cone-cylinder-cone in the close proximity of a flat plate. The interference flow field between these bodies was analyzed in detail. In this study, they used an implicit, approximately factored, central difference algorithm. They performed a steady state prediction of the flowfield at each instant step of the

separation process. In this study, they assumed that the flowfield adjusts quickly during the separation making the steady state computations acceptable at each instant.

Lohner [16] solved the problem of a two-dimensional object falling into a supersonic free stream using an adaptive remeshing technique. A grid, which was available to finite element method, was used to represent the mesh around the object placed in a cavity. Adaptive remeshing was performed every 100 iterations after a steady state solution was reached. The use of grid adapting proved beneficial in showing the changes in the strength and the location of shocks due to the motion of the object. In this study, the inviscid flow equations, which are inappropriate for cavity flows, are solved resulting in inaccurate solution. Also for multiple shock reflections, as in this case, shock-wave/boundary layer interaction becomes critical and viscous effects dominate in the region behind the first shock reflection.

Chesshire and Henshaw [17, 18] have developed a technique for the generation of curvilinear composite overlapped grids and numerical solutions of partial differential equations on them. Continuity conditions through interpolations are imposed at the overlapped boundaries. Their grid construction program, named CMPGRD, is used to create composite, two- and three-dimensional grids with any number of component grids, for finite difference and finite volume solvers. This program can generate a composite grid, which can be used for second or higher order spatial discretization with appropriate higher order interpolation. However, the higher order interpolations require a greater overlap region between subdomains and considerably more calculations. This program is also designed to generate automatically the sequence of coarser grids needed in a multigrid algorithm flow solvers.

Baysal et al. [19-21] incorporated the multigrid scheme with the CHIMERA method and accommodated these modifications to a finite volume solver. A cylinder was placed next to a flat plate and the overlapped grid was created by using a code that used grid-overlapping methodology. A steady state, upwind, finite volume solver was used and the interference flow field was studied. The details about the modification of CHIMERA and application cases are given in the reference [22]. Then, the overlapped scheme has been incorporated with the other domain

decomposition techniques, namely, the multiblock and zonal methods, to optimize the strength of the hybrid DDT [4].

Until recently, it has been difficult for the designer to predict numerically the flowfield about the complex, mutually interfering body configurations in the transonic speed regime. The geometric complexity of the grid generation and the existence of embedded regions of subsonic and supersonic flows that preclude the use of space marching codes have been major road blocks to the solution of the problem. With the advent of generalized, arbitrary geometry, multiblock grid codes [23], and sophisticated flow solvers [24] to work in accordance with these grids, good inviscid flow solutions can be obtained for very complex configurations such as fighter aircraft with external stores. Inviscid flow calculations have been successfully obtained on stores with multiple lifting surfaces [25, 26], multiple finned [27] and unfinned bodies [28, 29] and wing pylon unfinned store configuration [30] at low angles of attack. In addition, three-dimensional computations have been successfully obtained on overlapping and CHIMERA grids [31]. This method has been designed to simplify the grid generation and allow more timely and routine calculations of complex aircraft/store configurations. Steps in this direction have been taken by Benek [9] with multiple unfinned body calculations and by Meakin [14] with calculations on a wing unfinned body configurations.

After reviving relevant literature, it can easily be said that the interference flows have not been studied extensively especially in transonic speed regime. Because of being inherently nonlinear, transonic speed regime is very complicated and investigations in this regime generally bear very restrictive assumptions. Hence, there appears to be an urgent need for further and more comprehensive investigations, using both experimental and computational methods in this speed regime. In particular, interference flows encountered in external store carriage, especially store carriage and ~~separation.~~separation have not been computationally investigated extensively.

Biçimlendirilmiş: İki Yana Yasla, Girinti: Sol: 0 cm, Aralık Önce: 6 nk, Sonra: 6 nk

1.3 Objectives of the Present Work

Biçimlendirilmiş: Yazı tipi: 12 nk

Biçimlendirilmiş: Girinti: Sol: 0 cm

Accurate prediction of aerodynamic characteristics of store shapes is of paramount importance to the airframe designer. The accomplishment of the mission is highly dependent on engineers' ability to design an effective store shape with desirable aerodynamic qualities, both in free flight and interference flowfield. The interference flowfield, in which aerodynamic forces are generated by one or more of these external ~~stores,~~stores, has a great influence on the speed, range~~,~~ and endurance of modern fighters. Furthermore, the release of the store from the parent aircraft is highly dependent on its aerodynamic relationship with the wing or the body.

This relationship, or mutual interference, is mostly pronounced in the transonic speed regime where modern tactical fighters often operate. Transonic speed regime is very complicated because it is inherently nonlinear, and steady solution changes mathematical types, being elliptic in the subsonic portion of the flow and hyperb~~s~~ol~~n~~ic in the supersonic part of the flow.

The primary objective of the present work is to investigate the interference flowfield between an airfoil and a store combination by means of a CFD application in transonic speed regime. In such a complex flow, shock waves will exist and interact. Moreover, the airflow may separate due to angle of attack effects. Different locations of the store are also studied in order to understand how different store locations affect the interference flowfield. ~~Besides, t~~The effects of the change in angle of attack and store locations to the lift, drag~~,~~ and moment coefficients are investigated.

The grid overlapping method of DDT is used in order to investigate the interference flowfield between NACA64A010 airfoil and an Ogive Cylinder Ogive, which is placed under this airfoil. The two-dimensional solutions are obtained at different angles of attack and various store locations at 0.95 Mach. The C type, structured grids for airfoil and Ogive Cylinder Ogive are obtained independently and then, a two-dimensional composite overlapped grid from individual subdomain grids are created by means of the code MaGGiE [22].

A finite volume solver for the structured grids, a new version of CFL3D, ~~version~~ 6.0, is used as a flow solver. CFL3D has been developed primarily as a tool for external aerodynamics analysis. The original version of CFL3D was developed in the early 1980's in the Computational Fluids Laboratory at NASA Langley Center, ~~,~~ ~~H~~hence the name of the code, ~~which is~~ an acronym for the Computational Fluids Laboratory

Biçimlendirilmiş: Girinti: İlk satır: 0 cm

3-Dimensional flow solver. CFL3D can solve the time–dependent conservation law form of the Reynolds averaged Navier Stokes equations. The spatial discretization involves a semi discrete finite volume approach. Upwind biasing is used for the convective and pressure terms. Time advancement is implicit with the ability to solve steady or unsteady flows. Multigrid and mesh sequencing are also available for convergence acceleration. Moreover, numerous turbulence models are provided and multiple block topologies are possible with the use of one-–to-–one blocking, patching, overlapping, and embedding. However, CFL3D does not contain any grid generation software; thus, so that grids are supplied extraneously.

The Inviscid Euler equations are solved by implementing a steady state, implicit, approximately factored, upwind biased method at 0.95 Mach. The demonstration of cases is accomplished by plotting the Mach and pressure contours obtained at various angle of attacks and different store locations of two-dimensional flows. The steady state Cp distributions of the geometries and convergence histories of cases are also presented. BesidesAlso, the change in lift, drag, moment coefficients, and computation times of the cases are presented and discussed in this study.

2. MATHEMATICAL MODEL AND COMPUTATIONAL ALGORITHM

2.1 Governing Equations

The equations that govern fluid flow are mathematical interpretations of the physical laws that assure the conservation of mass, momentum and energy. These equations are known as the time dependent Navier-Stokes equations. The Navier-Stokes equations are reduced to the extensively used and very well known Euler equations if the viscosity, heat transfer and body forces are neglected for simplicity. In the present study, the Euler equations are expressed in their conservative form using the integral formulation. The three-dimensional, time-dependent Euler equations can be expressed in integral form as

$$\iiint_V \frac{\partial}{\partial t} Q dV + \iint_S \vec{E} \bullet \vec{h} dS = 0 \tag{2.1}$$

The expression of $\vec{E} \bullet \vec{h}$ represents the inviscid flux vectors normal to the boundary, and $\vec{h}$ is the unit normal vector pointing outward from the surface S, bounding the volume V. The inviscid flux vectors can be expressed as

$$\vec{E} = \{\vec{F}, \vec{G}, \vec{H}\} \tag{2.2}$$

The direct discretization of the integral form ensures the conservation of mass, momentum and energy at discrete levels. The conserved variables, represented as Q, are evaluated at cell centers and the fluxes, represented as $\vec{E}$, are evaluated at cell faces. Remaining valid in the presence of discontinuities in the flow; such as shocks and being tolerant to grid singularities can be accepted as the advantages of the finite volume formulation. Finite volume formulation is tolerant to grid singularities, because the flow equations are balanced over each cell of the grid. The analytical equivalent differential form of the governing equations may be obtained by applying Gauss's divergence theorem to the surface integral in equation (2.1). Therefore, the governing equations can be written in Cartesian Coordinates as

$$\frac{\partial Q}{\partial t}+\frac{\partial \vec{F}}{\partial x}+\frac{\partial \vec{G}}{\partial y}+\frac{\partial \vec{H}}{\partial z}=0 \tag{2.3}$$

In order to simplify the numerical treatment of boundary conditions for structured grids, the Euler equations are transformed into the boundary conforming curvilinear coordinates in ξ,η and ζ directions:

$$\frac{\partial \hat{Q}}{\partial t}+\frac{\partial \hat{F}}{\partial \xi}+\frac{\partial \hat{G}}{\partial \eta}+\frac{\partial \hat{H}}{\partial \zeta}=0 \tag{2.4}$$

The conserved variables and the inviscid fluxes can be expressed as

$$\hat{Q}=\frac{Q}{J}=\frac{1}{J}\begin{Bmatrix}\rho\\ \rho u\\ \rho v\\ \rho w\\ e\end{Bmatrix} \tag{2.5a}$$

$$\hat{F}=\frac{1}{J}\begin{Bmatrix}\rho U\\ \rho Uu+\xi_x p\\ \rho Uv+\xi_y p\\ \rho Uw+\xi_z p\\ (e+p)U-\xi_t p\end{Bmatrix} \tag{2.5b}$$

$$\hat{G}=\frac{1}{J}\begin{Bmatrix}\rho V\\ \rho Vu+\eta_x p\\ \rho Vv+\eta_y p\\ \rho Vw+\eta_z p\\ (e+p)V-\eta_t p\end{Bmatrix} \tag{2.5c}$$

$$\hat{H}=\frac{1}{J}\begin{Bmatrix}\rho W\\ \rho Wu+\zeta_x p\\ \rho Wv+\zeta_y p\\ \rho Ww+\zeta_z p\\ (e+p)W-\zeta_t p\end{Bmatrix} \tag{2.5d}$$

The adjusted contravariant velocities in curvilinear coordinates take the form and they are obtained from Cartesian coordinates by using the following transformation:

$$U = \xi_x u + \xi_y v + \xi_z w + \xi_t \tag{2.6a}$$

$$V = \eta_x u + \eta_y v + \eta_z w + \eta_t \tag{2.6b}$$

$$W = \zeta_x u + \zeta_y v + \zeta_z w + \zeta_t \tag{2.6c}$$

$$\xi = \xi(x, y, z, t), \eta = \eta(x, y, z, t) \text{ and } \zeta = \zeta(x, y, z, t) \tag{2.7}$$

The transformation metrics and Jacobean of transformation can be expressed as

$$\xi_x = J\left(y_\eta z_\zeta - z_\eta y_\zeta\right)$$

$$\eta_x = J\left(y_\zeta z_\xi - z_\zeta y_\xi\right)$$

$$\zeta_x = J\left(y_\xi z_\eta - z_\xi y_\eta\right) \tag{2.8a}$$

$$\xi_y = J\left(z_\eta x_\zeta - x_\eta z_\zeta\right)$$

$$\eta_y = J\left(z_\zeta x_\xi - x_\zeta z_\xi\right)$$

$$\zeta_y = J\left(z_\xi x_\eta - x_\xi z_\eta\right) \tag{2.8b}$$

$$\xi_z = J\left(x_\eta y_\zeta - y_\eta x_\zeta\right)$$

$$\eta_z = J\left(x_\zeta y_\xi - y_\zeta x_\xi\right)$$

$$\zeta_z = J\left(x_\xi y_\eta - y_\xi x_\eta\right) \tag{2.8c}$$

$$J = \frac{1}{\left(x_\xi\left(y_\eta z_\zeta - y_\zeta z_\eta\right) - x_\eta\left(y_\xi z_\zeta - y_\zeta z_\xi\right) - x_\zeta\left(y_\xi z_\eta - y_\eta z_\xi\right)\right)} \tag{2.8d}$$

The pressure and the enthalpy are related via the ideal gas law as

$$p = (\gamma - 1)\left[e_0 - \rho \frac{\left(u^2 + v^2 + w^2\right)}{2} \right] \tag{2.9a}$$

$$h_o = \frac{\gamma}{(\gamma - 1)} \frac{p}{\rho} + \frac{\left(u^2 + v^2 + w^2\right)}{2} \tag{2.9b}$$

2.2 Finite Volume Discretization

The finite volume formulation is based on the physical conservation laws in integral form for small volumes placed around every mesh point. Because of handling relatively arbitrary point distribution, the finite volume formulation has more flexibility than the finite difference method. Furthermore, the direct discretization of the integral form of conservation laws ensures the conservation of mass, momentum and energy at the discrete level. That is why the only requirement that must be added to the computational domain is to divide the computational domain into a finite number of non-overlapping volumes. However, the shape of these volumes is irrelevant which leads to no ambiguity at grid singularities.

A formulation for the semi-discrete approximation to the governing equations can be expressed as

$$V_i \frac{\partial Q_i}{\partial t} = -R_i \tag{2.10}$$

In this equation, Q represents the cell-averaged conserved variables and R_i represents the residual vector containing the inviscid fluxes.

For structured grid schemes, the summation is performed in the equation above over the six faces of the hexahedron, which defines the computational cell. Since structured grids have logical indexing of its cells, the following semi-discrete representation can be written as

$$\left(\frac{\partial \hat{Q}}{\partial t} \right)_{i,j,k} = -\frac{\hat{F}_{i+1/2,j,k} - \hat{F}_{i-1/2,j,k}}{\Delta\xi} - \frac{\hat{G}_{i,j+1/2,k} - \hat{G}_{i,j-1/2,k}}{\Delta\eta} - \frac{\hat{H}_{i,j,k+1/2} - \hat{H}_{i,j,k-1/2}}{\Delta\zeta} \tag{2.11}$$

In the equation above, the transformations are chosen so that the grid spacing in the computational space is uniform and of unit length, where $\Delta\xi = \Delta\eta = \Delta\zeta = 1$.

2.2.1 Upwind Method

The two methods that are used widely for the construction of the interface fluxes are the central differenced discretization and the upwind discretization of the right-hand side of the equation (2.10). The advantages of a central difference type discretization are that they are easier to code and take less memory than the upwind discretization. The drawbacks of these schemes are that they lack dissipation, are inherently unstable and decouple the adjacent cells. In order to counter these drawbacks, some artificial dissipation must be added for allowing shock capturing and suppressing even-odd point decoupling. The most popular dissipation formula is a blend of second and fourth order differences of the conserved variables by well-known "Jameson scheme" [32]. This type of dissipation requires user specified second and fourth order dissipation coefficients that have been found to be case dependent.

Upwind methods apply a discretization based on the locally one-dimensional propagation direction of waves. In other words, the interface fluxes are evaluated based on the characteristic theory for hyperbolic system of equations. This approach makes the scheme naturally dissipative. It is important to note that upwind differencing is actually equivalent to a central differencing plus an artificial dissipation term. Upwind methods are classified into two categories. One of them is flux vector splitting and the other one is flux difference splitting. A review of these schemes is given in reference [33].

In the present work, flux difference splitting of Roe [34], very well known Roe's scheme has been used to compute the inviscid fluxes. A discussion of this scheme is given in the next chapter.

2.2.2 Flux Difference Splitting

The basic philosophy behind the concept of flux difference splitting is to construct the cell interface fluxes through the solution of a set of Riemann problems. According to the upwind differencing proposed by Roe, the neighboring cells interact through discrete, finite amplitude waves. The amplitude and propagation speed of these waves are determined by solving the approximate Riemann problem. Roe's method seeks an exact solution to this approximate equation and distinguishes between the influence of the forward and backward moving waves. In other words, Roe's method seeks a solution to the locally one-dimensional Riemann problem

without sacrificing the nonlinear behavior of the interacting waves. Furthermore, Roe's method is based on extension of the linear wave decomposition, which is the exact linear solution to Riemann's problem, to the nonlinear equations.

Roe flux difference splitting is used to construct the upwind differences for the convective and pressure terms. If the eigenvalues of a flux Jacobean vanishes, the corresponding eigenvalues of the dissipation matrix also vanishes. This leads to a one or two-cell resolution of discontinuities such as shocks. For example, the spatial derivative can be written conservatively in the ξ direction as a flux balance across a cell as

$$\left(\frac{\partial E}{\partial \xi}\right)_i = \left(E_{i+1/2} - E_{i-1/2}\right)/\left(\xi_{i+1/2} - \xi_{i-1/2}\right) \tag{2.12}$$

The subscript of the first variable refers to a cell center; i+1/2 and i-1/2 correspond to cell faces. The interface flux is determined from a state variable interpolation and a locally one-dimensional model of wave interactions normal to the cell interfaces. According to the Roe's scheme, the flux across each cell face is evaluated by using the numerical flux equation.

$$E_{i+1/2} = \frac{1}{2}\left[E(Q_L) + E(Q_R) - \left|\tilde{A}\right|(Q_R - Q_L)\right]_{i+1/2} \tag{2.13}$$

In equation (2.14), Q_L and Q_R are the conserved variables to the left and right of the interface and $\tilde{A}$ is the Roe-averaged flux Jacobean matrix. The term $\left|\tilde{A}\right|(Q_R - Q_L)$ is the dissipation term contributing to the interface flux.

The implementation of Roe's scheme to solve the nonlinear Euler equations requires a linearization of the Euler equations because the Roe's scheme is based on the linear concepts. Linearization of the Euler equations is accomplished by evaluating the Jacobean matrix A, with the averaged quantities donated by (~) sign.

$$\tilde{\rho} = \sqrt{\rho_L \rho_R} \tag{2.14a}$$

$$\tilde{u} = \left(u_L + u_R\sqrt{\frac{\rho_R}{\rho_L}}\right)/\left(1 + \sqrt{\frac{\rho_R}{\rho_L}}\right) \tag{2.14b}$$

$$\tilde{v} = \left(v_L + v_R \sqrt{\frac{\rho_R}{\rho_L}} \right) / \left(1 + \sqrt{\frac{\rho_R}{\rho_L}} \right) \tag{2.14c}$$

$$\tilde{w} = \left(w_L + w_R \sqrt{\frac{\rho_R}{\rho_L}} \right) / \left(1 + \sqrt{\frac{\rho_R}{\rho_L}} \right) \tag{2.14d}$$

$$\tilde{h}_0 = \left(h_{0L} + h_{0R} \sqrt{\frac{\rho_R}{\rho_L}} \right) / \left(1 + \sqrt{\frac{\rho_R}{\rho_L}} \right) \tag{2.14e}$$

$$\tilde{a}^2 = (\gamma - 1) \left[\tilde{h}_0 - \frac{\left(\tilde{u}^2 + \tilde{v}^2 + \tilde{w}^2 \right)}{2} \right] \tag{2.14f}$$

The Roe-averaged Jacobean matrix $\tilde{A}$ is the mean value of the Jacobean matrix A with the following properties:

1. The Roe-averaged Jacobean matrix $\tilde{A}(Q_L, Q_R)$ approaches true Jacobean matrix A as Q_L and Q_R approach Q.

2. The flux difference between left and right states can be written as

$$\tilde{A}(Q_L, Q_R)(Q_R - Q_L) = E(Q_R) - E(Q_L) \tag{2.15}$$

3. $\tilde{A}$ has a complete set of real eigenvalues and vectors.

The first property ensures the consistency of the governing differential equations. The second property satisfies the Rankine-Hugoniot shock jump condition. The second property is also responsible for the improved resolution of shocks and contact discontinuities. The final property allows the matrix $\tilde{A}$ to be expressed in the canonical form as

$$\tilde{A} = \tilde{\Gamma} \Lambda \tilde{\Gamma}^{-1} \tag{2.16}$$

The columns of $\tilde{\Gamma}$ are the right eigenvectors of $\tilde{A}$, and the rows of $\tilde{\Gamma}^{-1}$ are the left eigenvectors $\tilde{A}$. A diagonal matrix comprising of eigenvalues of $\tilde{A}$ can be defined as Λ. So that, the flux difference can be expressed as

$$E(Q_R) - E(Q_L) = \tilde{\Gamma} \Lambda \tilde{\Gamma}^{-1} \Delta Q = |\Delta E_1| + |\Delta E_2| + |\Delta E_3| \tag{2.17}$$

$$\left|\Delta E_1\right| = \left|\tilde{U}\right|\left\{\left(\Delta\rho - \frac{\Delta p}{\tilde{a}^2}\right)\begin{bmatrix} 1 \\ \tilde{u} \\ \tilde{v} \\ \tilde{w} \\ \dfrac{\tilde{u}^2+\tilde{v}^2+\tilde{w}^2}{2} \end{bmatrix} + \begin{bmatrix} 0 \\ \Delta u - \Delta U n_x \\ \Delta v - \Delta U n_y \\ \Delta w - \Delta U n_z \\ \tilde{u}\Delta u + \tilde{v}\Delta v + \tilde{w}\Delta w - \tilde{U}\Delta U \end{bmatrix}\right\} \tag{2.18a}$$

$$\left|\Delta E_{2,3}\right| = \left|\tilde{U} \pm \tilde{a}\right|\left(\frac{\Delta p \pm \tilde{\rho}.\tilde{a}\Delta U}{2\tilde{a}^2}\right)\begin{bmatrix} 1 \\ \tilde{u} \pm \tilde{a}n_x \\ \tilde{v} \pm \tilde{a}n_y \\ \tilde{w} \pm \tilde{a}n_z \\ \tilde{h}_0 \pm \tilde{a}\tilde{U} \end{bmatrix} \tag{2.18b}$$

In equations (2.19a) and (2.19b), ΔU and the Roe-averaged contravariant velocity can be expressed as $\Delta U = \Delta u n_x + \Delta v n_y + \Delta w n_z$ and $\tilde{U} = \tilde{u}n_x + \tilde{v}n_y + \tilde{w}n_z$ respectively.

2.3 Time Integration

Time integration may be done either explicitly or implicitly. In the explicit method, the matrix of unknown variables that are formed at the new time level is a diagonal matrix and the right hand side of the system depends on only the flow variables from the previous level. The explicit method has many advantages; it requires fewer arithmetic operations per time step, it is simple to code and it can be vectorized easily. On the other hand, the main drawback of this method is to stem from the severe restrictions imposed on the maximum allowable time step due to the stability and convergence conditions.

Implicit methods traditionally have high computational costs per iteration in terms of both CPU time and memory. In other words, the number of the arithmetic operations required per time step is higher than the explicit scheme, but this drawback is counterbalanced by implicit schemes pose no theoretical limitation on the time step. There is more than one set of unknown variables at the same time level; hence, the matrix to be inverted is not a diagonal one. Thus, the extra work required for the implicit scheme is usually offset by the advantages obtained by the

increased stability limits. On the other hand, explicit methods are relatively inexpensive per iteration but have restrictions on stability.

The capacity of the computer used and the physics of the flow problem to be simulated also must be investigated before making a decision about the type of the time integration scheme. For instance, most of the supercomputers that are used today have high-speed vector processors; however, the degree of a certain algorithm, which is vectorized, can be critical. Although explicit schemes can be vectorized easily, the implicit schemes need substantial amount of memory for temporary storage for data and need management to become completely vectorized.

It is important to note that, for unsteady flow problems, time accuracy of the numerical solution is required and the temporal conservation error diminishes with decreasing time step. Both implicit and explicit methods are capable of computing time accurate solutions, but time scales are usually so small that the stability of the explicit methods is not jeopardized. Hence, on a per iteration basis, explicit methods appear to be the most convenient and economical approach for time accurate unsteady simulations and implicit methods for steady state calculations.

The details of the time integration schemes for the structured grid algorithm, as implemented in the computer code CFL3D [35], will be presented in the following paragraphs. The structured grid algorithm used in this study advances the solution in time by using an implicit method. This may be accomplished by linearizing the inviscid fluxes in time.

$$\hat{E}^{n+1} = \hat{E}^{n} + \frac{\partial \hat{E}^{n}}{\partial Q} \Delta Q^{n} \tag{2.19}$$

For steady state calculations, the governing equations are integrated from an arbitrary initial condition to a time-asymptotic state. Thus, when a steady state solution is desired, it is typical to employ first order time accurate schemes and use non time-like maneuvers in an attempt to accelerate the algorithm. Some examples of current convergence acceleration techniques are local time stepping [32], mesh sequencing, multigrid technique [36, 37] and implicit residual smoothing [32, 34].

The local time stepping can be viewed as a means of conditioning the coefficient matrix in implicit schemes or interpreted as an attempt to use a uniform Courant

number throughout the flow field for explicit schemes. In mesh sequencing technique, it used a good initial guess for a fine mesh by iterating on a sequence of coarser meshes. In multigridding, it is dumped the low frequency errors by using a series of coarser grids constructed from the fine mesh. Finally, in implicit residual smoothing technique, the averages of the residuals are used like implicit schemes.

All the above techniques have been found to accelerate the convergence to steady state. Local time stepping, mesh sequencing and the multigrid technique are available options in the structured grid code called CFL3D, whereas local time stepping and implicit residual smoothing are the options of unstructured grid code that is USM3D.

Applying the Euler implicit time integration to equation (2.4) yields

$$\frac{\Delta Q}{\Delta t} + \delta_\xi F^{n+1} + \delta_\eta G^{n+1} + \delta_\zeta H^{n+1} = 0 \tag{2.20}$$

In the equation above, n donates the time level. The inviscid fluxes can also be linearized as

$$\delta_\xi (F)^{n+1} = \delta_\xi (F)^n + \delta_\xi \frac{\partial (F)^n}{\partial Q} \Delta Q \tag{2.21a}$$

$$\delta_\eta (G)^{n+1} = \delta_\eta (G)^n + \delta_\eta \frac{\partial (G)^n}{\partial Q} \Delta Q \tag{2.21b}$$

$$\delta_\zeta (H)^{n+1} = \delta_\zeta (H)^n + \delta_\zeta \frac{\partial (H)^n}{\partial Q} \Delta Q \tag{2.21c}$$

Putting the equations above into the equation (2.21) results in the following expression:

$$\left[\frac{I}{\Delta t} + \delta_\xi \frac{\partial F}{\partial Q} + \delta_\eta \frac{\partial G}{\partial Q} + \delta_\zeta \frac{\partial H}{\partial Q} \right]^n \Delta Q = -\left[\delta_\xi F + \delta_\eta G + \delta_\zeta H \right]^n = -R^n \tag{2.22}$$

Equation (2.23) forms a system of algebraic equations. The coefficient matrix is banded and the bandwidth depends on the grid size and choice of spatial differencing method. The left-hand side requires an inversion of a very large matrix. The exact

inversion of the matrix is very close due to the large number of operations and computer memory required. An approximate factorization scheme splits the implicit operator into a sequence of easily inverted equations. The spatial split, three-factor approximate factorization of Beam and Warming [38] that is applied to equation (2.23) yields

$$\left[\frac{I}{\Delta t}+\delta_{\xi}\frac{\partial F}{\partial Q}\right]^{n}\times\left[\frac{I}{\Delta t}+\delta_{\eta}\frac{\partial G}{\partial Q}\right]^{n}\times\left[\frac{I}{\Delta t}+\delta_{\zeta}\frac{\partial H}{\partial Q}\right]^{n}\times\Delta Q\cong -R^{n}\times\left(\Delta t\right)^{2} \tag{2.23}$$

or

$$\left[\frac{I}{\Delta t}+\delta_{\xi}\frac{\partial F}{\partial Q}\right]^{n}\Delta Q^{**}=-\left(R^{*}\right)^{n} \tag{2.24a}$$

$$\left[\frac{I}{\Delta t}+\delta_{\eta}\frac{\partial G}{\partial Q}\right]^{n}\Delta Q^{*}=\left(\frac{I}{\Delta t}\right)\Delta Q^{**} \tag{2.24b}$$

$$\left[\frac{I}{\Delta t}+\delta_{\zeta}\frac{\partial H}{\partial Q}\right]^{n}\Delta Q=\left(\frac{I}{\Delta t}\right)\Delta Q^{*} \tag{2.24c}$$

$$Q^{n+1}=Q^{n}+\Delta Q \tag{2.24d}$$

This scheme requires the solution of a 5×5 block tridiagonal system. It has the advantage of being fully vector form. The present implementation takes advantage of the large memory available in the current supercomputers by creating long data vectors that, in turn, result in faster processing rates. However, employing the approximate diagonal form of the spatial vectors can be resulted in the saving of time. Each of the spatial factors is approximated with a diagonal inversion as

$$\left[\frac{1}{J\Delta t}+\delta\frac{\partial E}{\partial Q}\right]^{n}\Delta Q^{*}\cong\tilde{\Gamma}\left[\frac{1}{J\Delta t}+\delta^{-}\Lambda^{+}+\delta^{+}\Lambda^{-}\right]\tilde{\Gamma}^{-1}\Delta Q^{*} \tag{2.25}$$

The diagonal matrix Λ is the matrix of eigenvalues of A. Because of the repeated eigenvalues of matrix, only scalar diagonal inversions rather than block inversions are used in each direction.

2.4 Initial and Boundary Conditions

The solution of any partial differential equation is completely depending on the choices of initial and boundary conditions. The initial conditions should correspond to the physical nature of the flow. As expected, different form of such conditions must be used for steady and unsteady calculations.

Two types of boundary condition representations are employed in CFL3D, namely, cell-center and cell-face. For cell-center type boundary conditions, the flow field variables are specified at "ghost" points corresponding to two cell center locations analytically extended outside the grid. For cell-face type boundary conditions, the flow field variables and their gradients are specified at the cell face boundary [39].

The initial conditions for the steady state calculations may be arbitrary. However, a good initial guess, which is obtained from experiments, empirical relations, theories or previous computational results for the flow field, ultimately reduces the CPU time required to converge the solution. That is why it is commonly used for steady flows to choose free stream conditions as the initial conditions. As in the initial conditions, the free stream Mach number of 0.95 and the free stream temperature of 460 degrees Rankin are applied for all the cases.

The free stream boundary conditions are cell-center type boundary conditions. The flow field variables for both sets of ghost points are set equal to the initial values, which are:

$$\rho_{initial} = 1.0 \tag{2.26a}$$

$$u_{initial} = M_{\infty} \cos\alpha \cos\beta \tag{2.26b}$$

$$v_{initial} = -M_{\infty} \sin\beta \tag{2.26c}$$

$$w_{initial} = M_{\infty} \sin\alpha \cos\beta \tag{2.26d}$$

$$p_{initial} = \rho_{initial}(a_{initial})^2 / \gamma \tag{2.26e}$$

It should be noted that all boundary conditions used in this study are specified explicitly. The walls are considered impermeable and adiabatic. The far field boundary conditions are incorporated by using locally one-dimensional characteristic

boundary conditions. The velocity normal to the boundary and the speed of sound for each cell are calculated from the locally one-dimensional Riemann invariants, that is

$$R^{\pm} = U \pm \frac{2}{\gamma - 1} a \tag{2.27}$$

The invariants, for example in ξ direction, are constant along the characteristics defined as

$$\left(\frac{d\xi}{dt}\right)^{\pm} = U \pm a \tag{2.28}$$

These invariants are used to calculate the local normal velocity and the speed of sound. The local normal velocity and the speed of sound at the boundaries are calculated by adding or subtracting the two Riemann invariants respectively. The local normal velocity is calculated by summing and the speed of sound is calculated by subtracting them. Other quantities such as density and pressure can be found by using the entropy relation and the equation of state respectively. For steady inviscid flows, the velocity components used in the surface boundary conditions and the contravariant velocity, which is U, can be expressed as

$$u_{wall} = u_{center} - n_x U \tag{2.29a}$$

$$v_{wall} = v_{center} - n_y U \tag{2.29b}$$

$$w_{wall} = w_{center} - n_z U \tag{2.29c}$$

$$U = \vec{V} \bullet \hat{n} = u n_x + v n_y + w n_z \tag{2.30}$$

The entropy is determined using the value from outside the domain for the inflow and from inside the domain for outflow. The entropy and speed of sound are used to determine the density and pressure on the boundary. The pressure for the boundary conditions can be obtained by extrapolation from the interior point value that is order of zero. The density is then calculated by employing the state equation [40, 41]. The outer boundary conditions of the grids are shown in the figure 2.1 and figure 2.2.

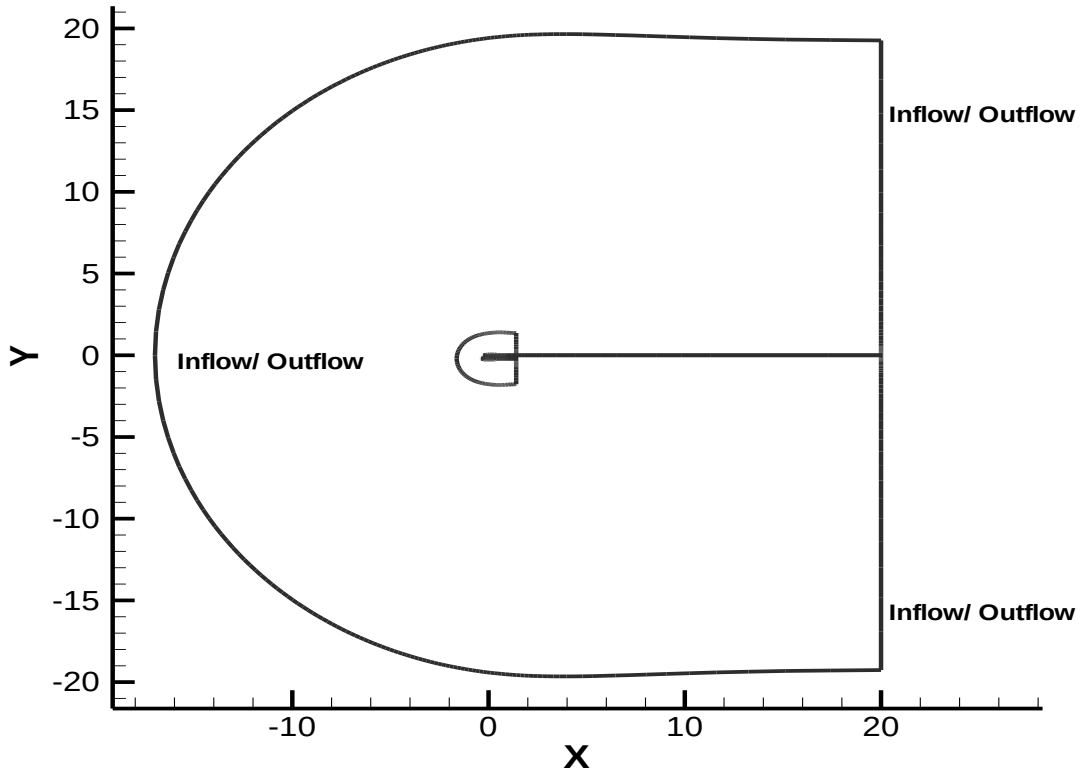

Figure 2.1. Outer boundary conditions for grid one

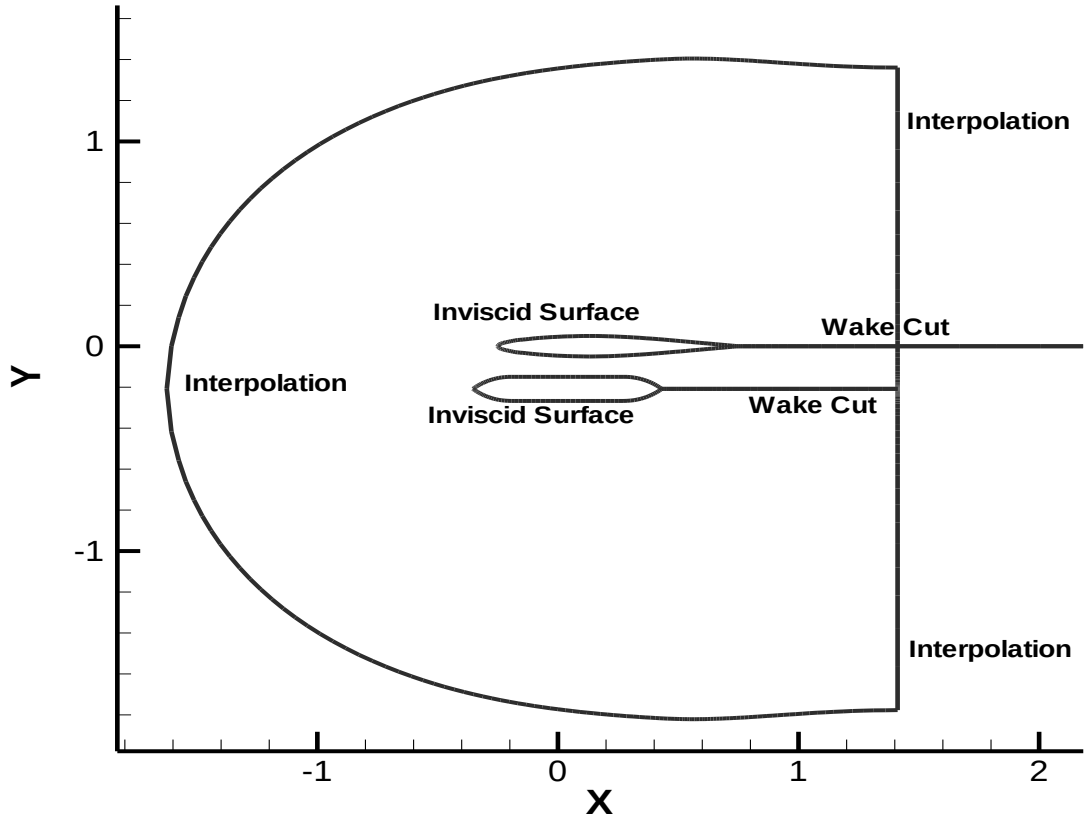

Figure 2.2. Outer boundary conditions for grid two

2.5 MaGGiE: A Domain Decomposition Methodology

Grid overlapping, also known as the overset grid or CHIMERA technique, requires neither one to one connectivity or nor a shared interface to pass flow information from one grid to another. With this method, a variety of grid topologies can be used together. The CHIMERA implementation used in CFL3D is based on the method of Benek et al. [10].

The construction of the overlapped grid for the present study is accomplished by the MaGGiE code presented in [21, 22]. This technique is based on the CHIMERA grid scheme of Stager et al. [7-10]. The CHIMERA algorithm discretizes the subdomain using finite difference method and solves the flow equations on the composite grid utilizing a central difference scheme. Baysal et al. [21] modified the composite grid generation of this scheme. This modified scheme is named MaGGiE, for Multi Geometry Grid Embedder. MaGGiE discretizes the subdomain using a finite volume method as well as finite difference method. It is also capable of constructing the composite grid at coarser grid levels. The resulting composite grid is then well suited for the finite volume solver, which is CFL3D. It should be noted that the composite grid is defined here as the union of subdomain grids overlapped on one another.

The program MaGGiE creates two- or three-dimensional composite grids from individual subdomain grids. It also provides the necessary information for the intergrid communication. The subdomain grids create holes in other subdomain grids in which they are overlapped. The main idea behind the holes is that the grid points, which belong to base grid, are excluded from the solution of the subdomain grid. This procedure is repeated for all of the holes in the composite grid. In order to obtain a logical sequence of grid communication between overlapped grids, a form of hierarchy is needed. An order of hierarchy is formed between the grids allows the interaction of appropriate grids, simplifies the development of the data structure required for this interaction and limits the search to locate points in other grids for the purpose of interpolation. The MaGGiE code is divided into six stages. The first three stages are used to acquire fine level grid communication data and the last three stages are used to acquire overlapped grid communication data.

MaGGiE’s composite grid generation consist of establishing the proper lines of communication among the grids through appropriate data structure and constructing

holes within grids. Moreover, MaGGiE identifies points with holes and illegal zones, locates points from which outer and whole boundary values can be interpolated, and evaluates interpolation parameters. Since the grids cover the same area for overlapping, computations on the grids in this area would be redundant. Therefore, certain points on the base grid will be eliminated from the computation. The other grid is used to carve a “hole” in the base grid. Any cell center point of the base grid located within this hole is designated a “hole point.” The “nonhole” cell center points of the base grid that border hole points both vertically and horizontally are labeled “fringe points.” The remaining grid points that have not been designated as either hole or fringe points are called “field” points [39].

A searching algorithm is used to identify the particular eight points that define the hexahedral target cell. The search begins with an initial guess for the target cell. Next, the current target cell is isoparametrically mapped into a unit cube in computational space. The same transformation into the mapped coordinate system is applied to the fringe point; if the mapped fringe point lies in the same unit cube as the current target cell, then that target cell in fact encases the fringe point. If the mapped fringe point lies outside the unit cube, then the current target cell is not the correct choice. However, the magnitude and the direction of the mapped fringe point relative to the current target cell may be used to choose a new guess for the target cell. The mapping process is repeated until the correct target cell is identified. With the correct target cell identified, the data are transferred from the target cell to the fringe point with trilinear interpolation in computational space. Outer boundary values of the polar grid are determined in a similar manner. The MaGGiE code, written specifically for CFL3D by Baysal et al. [21], can determine the interpolation information between grids.

3. RESULTS AND DISCUSSION

3.1 Geometry and Grid Generation

The geometries used in this study ~~are~~ consist~~ing~~ of an airfoil that is NACA64A010 and an "ogive cylinder ogive" ~~or namely (OCO~~O ~~CO)~~. The geometry of an airfoil is very important in transonic speed regime. The airfoil ~~has to~~must have a significantly better transonic performance as ~~it is~~ compared to the other airfoils. Today, there are many supercritical airfoils that~~, which have the better~~ perform better~~ance~~ than the ~~rest of the~~other airfoils in transonic speed regime. However, although the NACA6A series airfoils are widely used in transonic and supersonic applications, they are actually designed to attain laminar boundary layer flow over a portion of the airfoil. Essentially, the expected performance of a transonic airfoil is to control the expansion of the flow to supersonic speed and its subsequent recompression. Many experimental and CFD studies have shown that NACA64A010 has a good performance in transonic speed regime [42], and it was used in this study.

An "o~~O~~give nose cylinder" (ONC)~~or namely ONC~~ is commonly used by aeronautics and astronautics engineers in order to represent the external store of a flying object in CFD problems. In fact, the geometry of the external store used in this study is an "ogive cylinder ogive"~~. B~~ because~~,~~ the geometry of this external store has a fines ratio of 6.667 and the front and back parts have the same size of calibers, which is 1.333. The dimensions and the lengths used in the geometries are nondimensionalized for simplicity by the thickness of the o~~O~~give ~~C~~cylinder o~~O~~give, that is, "d."~~:~~ The geometry of the ~~OCO~~ OCO is shown in figure 3.1. Initially, the ~~OCO~~ OCO is located in the carriage position, 1.77 diameters below the airfoil, and one diameter in front of the airfoil. Then different locations of ~~OCO~~the OCO are studied. The initial case~~s~~ position of ~~OCO~~the OCO with respect to NACA64A010 is shown in ~~the~~ figure 3.2. A special code is used to position the geometries and grids with respect to each other. Then, by using another code, these two individual

Biçimlendirilmiş: Yazı tipi: 12 nk
Biçimlendirilmiş: Sola
Biçimlendirilmiş: Yazı tipi: 12 nk
Biçimlendirilmiş: Girinti: Sol: 0 cm
Biçimlendirilmiş: Girinti: İlk satır: 0 cm

subdomain grids are transferred in a form that MaGGiE code can read the required grid data to create an overlapped grid.

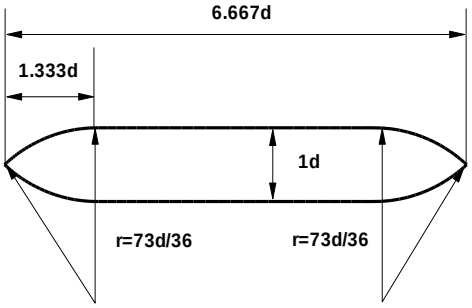

Figure 3.1.÷ Ogive Cylinder Ogive geometry

Biçimlendirilmiş: Sola

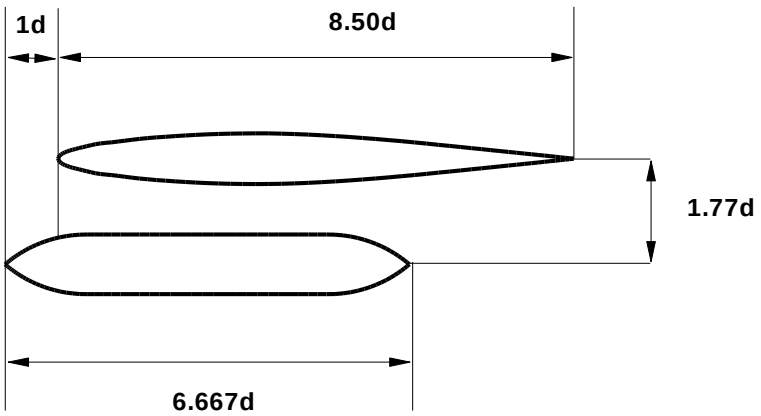

Figure 3.2.÷ Ogive Cylinder Ogive relative position

Biçimlendirilmiş: Sola

Biçimlendirilmiş: Girinti: İlk satır: 0 cm

The first step in solving a CFD problem is to decide geometry and create a grid that is available to the code that an engineer performs the calculations. The objective of grid generation is to identify the location of the grid points in the computational domain and the location of the corresponding points in the physical space. Typically, grid generation schemes can be categorized as algebraic and differential methods. In this study, the algebraic structured type grids are generated and used. Mainly, this type of grid is easy to create and very fast computationally. In addition~~Besides~~, the ability to cluster grid points in different regions can be easily implemented. The flow

solver, CFL3D, does not contain any grid generation software, so that the structured type grids are generated extraneously for the geometries.

The grids consist of separate single grid zones with “C type” grids. The grids generated for airfoil and ~~OCO~~the OCO are composed of 25498 and 17138 points respectively. An elliptic grid generator was used in order to generate the grids. Elliptic grid generators work very well for the domains where all the physical boundaries are specified and closed. The radius of the grid generated for the airfoil has thirteen chord lengths, which is one hundred and ten diameters of the ~~OCO~~~~the~~ OCO. On the other hand, the grid radius of the ~~OCO~~ OCO has two chord lengths, and which is approximately thirteen diameters of the ~~OCO~~ OCO. The general and detailed grids are shown for the geometries in ~~the~~ figures 3.3a, 3.3b, 3.4a~~,~~ and 3.4b.

The composite grid generation starts with the subdomain grids being translated and rotated to their proper locations relative to fixed global origin. A special code mentioned before is used for this purpose. In order to prevent misunderstanding, the individual subdomain grids are given names. The grid, which is used for NACA64A010 airfoil is named “grid one” and the other grid, which is used for Ogive Cylinder Ogive, is named “grid two.”~~.~~ First, the ~~OCO~~ OCO and its grid are positioned relative to the airfoil grid and then the program MaGGiE is executed in order to obtain the composite grid. MaGGiE’s composite grid generation consists of establishing the proper lines of communication among the grids through appropriate data structure and constructing holes within grids. Moreover, MaGGiE identifies points with holes and illegal zones, locates points from which outer and hole’s boundary values can be interpolated, and evaluates interpolation parameters.

A two-dimensional composite grid is created by the program MaGGiE from individual subdomain grids and the necessary intergrid communication is provided. The both subdomain grids create holes within each other in which they are overlapped. In the holes, base grid points are excluded from the solution. In other words, since the grids cover the same area for overlapping, computations on the grids in this area would be redundant. Therefore, certain points on the base grids are eliminated from the computation. The overlapped grid is used to carve a “hole” in the base grid and these grid points are used in the solution. Any cell center point of the base grid located within this hole is designated a “hole point.”~~.~~ The “nonhole” cell center points of the base grid, which border points defined as holes both

vertically and horizontally, are labeled “fringe points.”. The remaining grid points that have not been designated as either hole or fringe points are called “field” points.

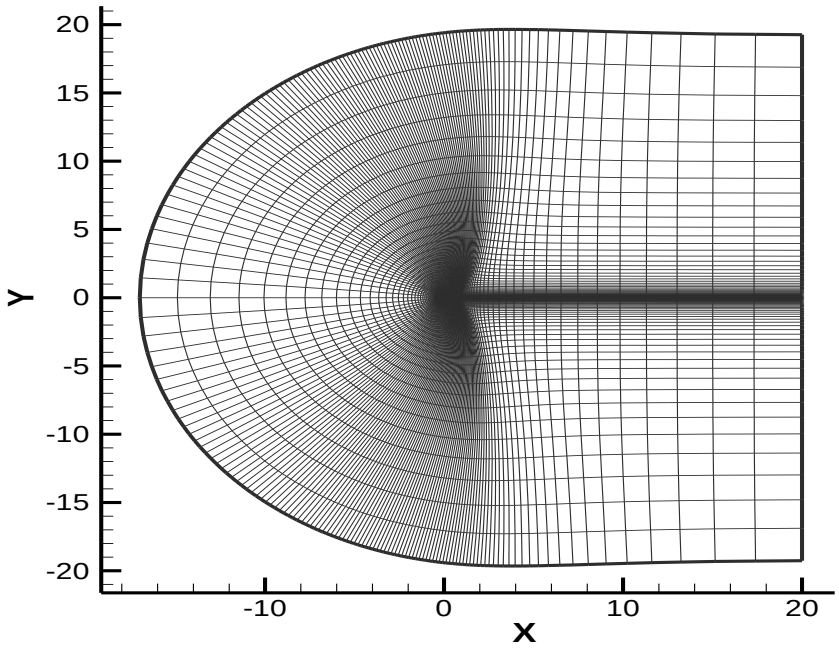

Figure 3.3.a. C type grid for NACA64A010 aAirfoil

Biçimlendirilmiş: Sola

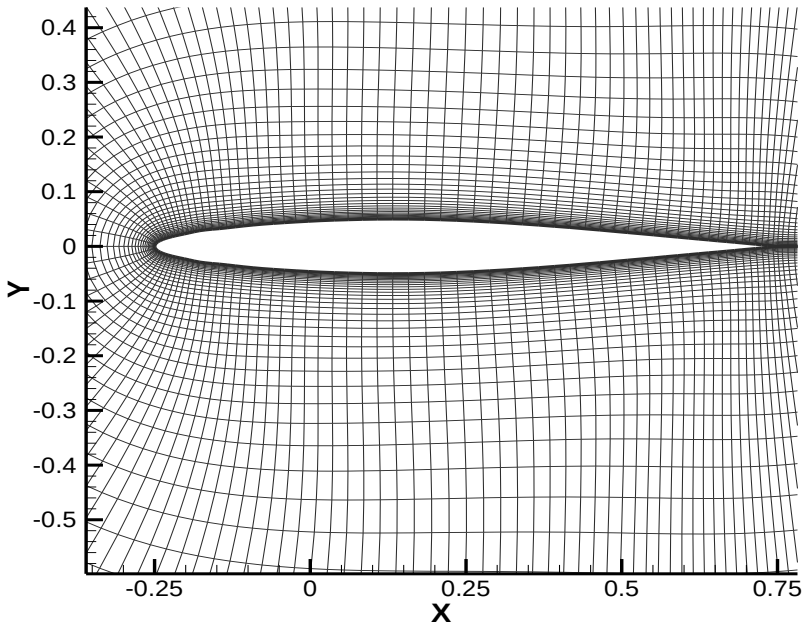

Figure 3.3.b.: Detailed C type grid for NACA64A010 a.Airfoil

Biçimlendirilmiş: Sola

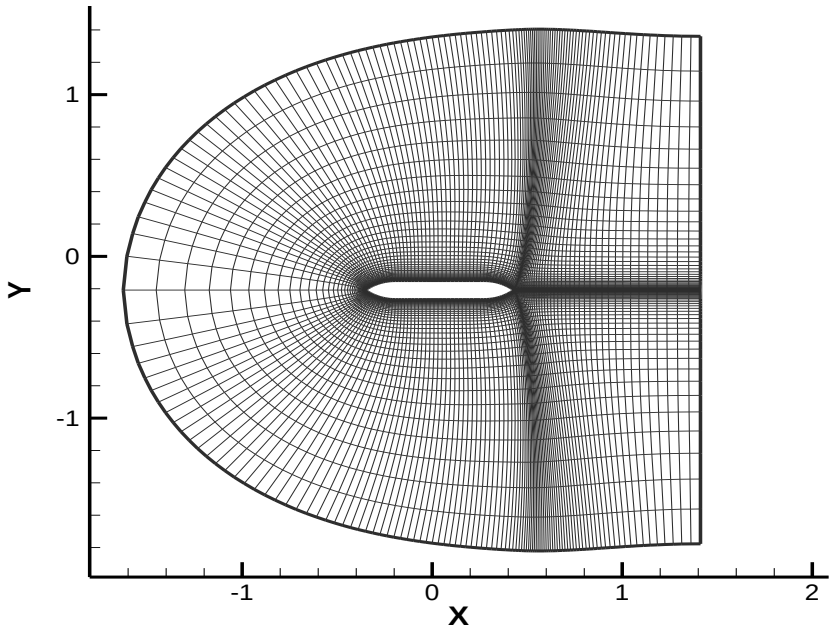

Figure 3.4.a.: C type grid for Ogive Cylinder Ogive

Biçimlendirilmiş: Sola

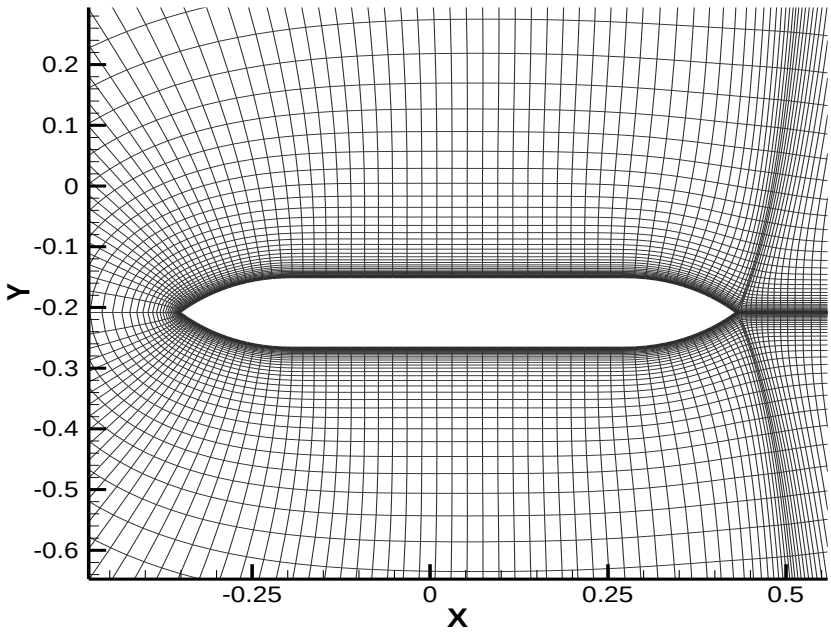

Figure 3.4.b.: Detailed C type grid for Ogive Cylinder Ogive

Biçimlendirilmiş: Sola

Biçimlendirilmiş: Girinti: İlk satır: 0 cm

The communication between the hole and fringe points is provided by interpolated points, which can be a member of any grids used in the composite form. The outer grid points of grid two, which is shown with diamonds in figure 3.5, are "interpolated points" determined for grid two. These interpolated boundary points are created by MaGGiE, because no boundary conditions are applied at the outer part of grid two.

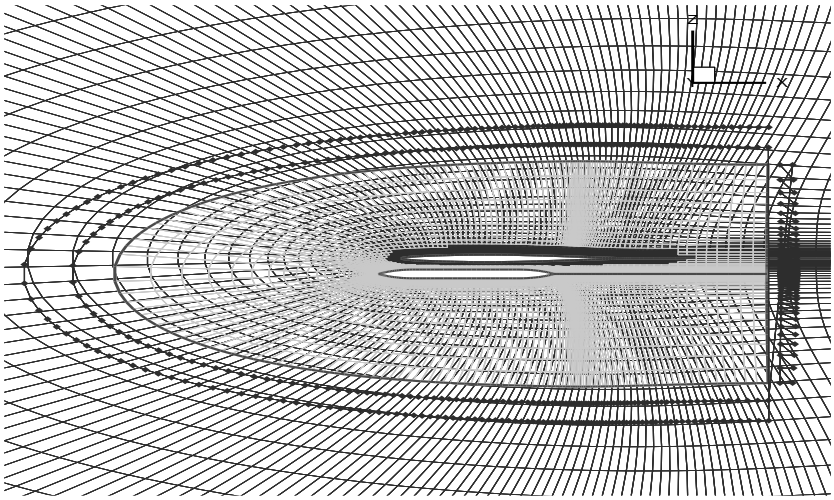

Figure 3.5.~~:~~ Interpolated boundary points of grid two

Biçimlendirilmiş: Sola

Biçimlendirilmiş: Girinti: İlk satır: 0 cm

In order to obtain a logical sequence of grid communications between overlapped grids, a form of grid hierarchy is needed. The order of hierarchical form between the grids allows the interaction of appropriate grids, simplifies the development of the data structure required for this interaction, and limits the search to locate points in other grid for the purpose of interpolation. The program MaGGiE determines the stencils for the fringe points of grid one and grid two. For example, for the first three cases, there are 174 fringe points of grid one, which are interpolated from grid two. Similarly, there are 282 fringe points of grid two, which are interpolated from grid one. Especially~~,~~ at the outer boundary of grid two, no boundary conditions are applied and the outer part of grid two is used for the purpose of interpolation from grid one. There are 576 boundary points in grid two for which stencils must be determined and these points are interpolated from grid one. The total number of cells is~~are~~ 20800 and the total number of grid points is~~are~~ 42636, where 577 ~~of them~~ are hole points and 456 ~~of them~~ are fringe points in the composite grid.

The width of the overlapped region is dependent on the width of the interpolation formula used in the MaGGiE code, the stencil of the spatial differencing~~,~~ and the smoothness of the cells. If there is too much overlap between subdomains, this overlapped region results in unnecessary duplication of computations in these regions and too little overlapped region results in illegal or lack of communications between subdomains. Five~~-~~ or ten~~--~~cell~~s~~ overlap is found to be efficient for finest

level grids [22]. The objective is to create each subdomain grid independently in such a manner that when one grid is overlapped within another the cell sizes of both grids are of the same order within the overlapped region. This is not a necessary condition; however, the transference of data from one grid to another through interpolation becomes more accurate when the grid sizes are closer. The accuracy improves for similar cell sizes because most interpolations functions are weighted by physical distances and not percentage of cell volumes.

In this study, it is taken into consideration and the grids in the overlapped regions are not too much or too little. If there is too much or too little overlap between subdomains, MaGGiE code cannot perform interpolation procedure at these grid points. In order to calculate these inappropriate overlapped points, MaGGiE code defines some extra points away from overlapped region, which are called "extrapolated points." As a result, these inappropriate points are calculated from these extra points. These extra points, which are used for extrapolation procedure, may cause erroneous results and MaGGiE code always warns users about it and usually does not give permission to run the flow solver. Although the user runs the code, the code usually blows-up after some certain time steps and prevents the user to reach erroneous results. In each case, there are no extrapolated points in the overlapped region. Holes that are created in this overlapped region, "hole one" and "hole two," are shown in figures 3.6.a and 3.6.b respectively. Moreover, for subdomain grids, which in general overlap each other in an irregular fashion, it is desirable to use conservative interface procedure. Such an idea helps, for example, finding the correct shock location for shocks passing through grid boundaries, and ensures artificial shocks are not generated at the grid interfaces. The code can alleviate this drawback and help the user to reach the most correct results after the calculations.

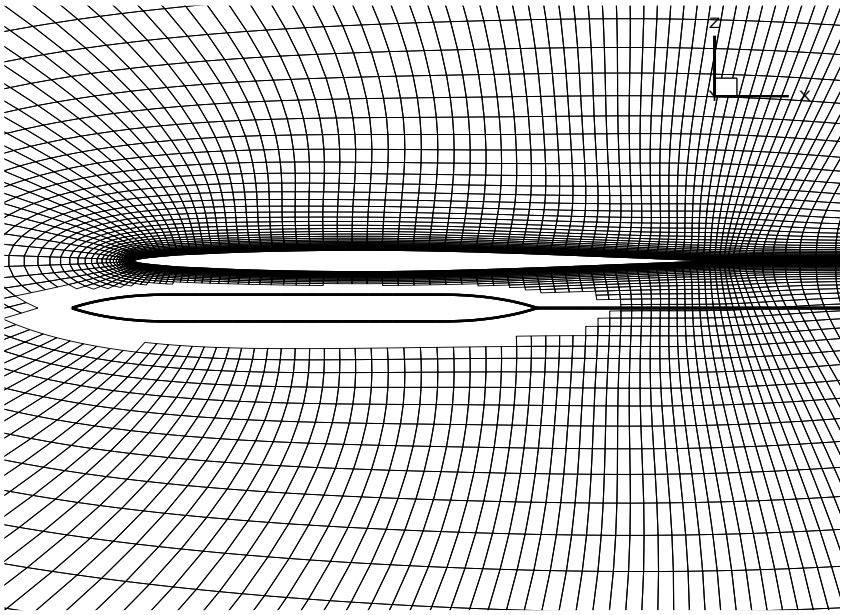

Figure 3.6.a.÷ Hole one

Biçimlendirilmiş: Sola

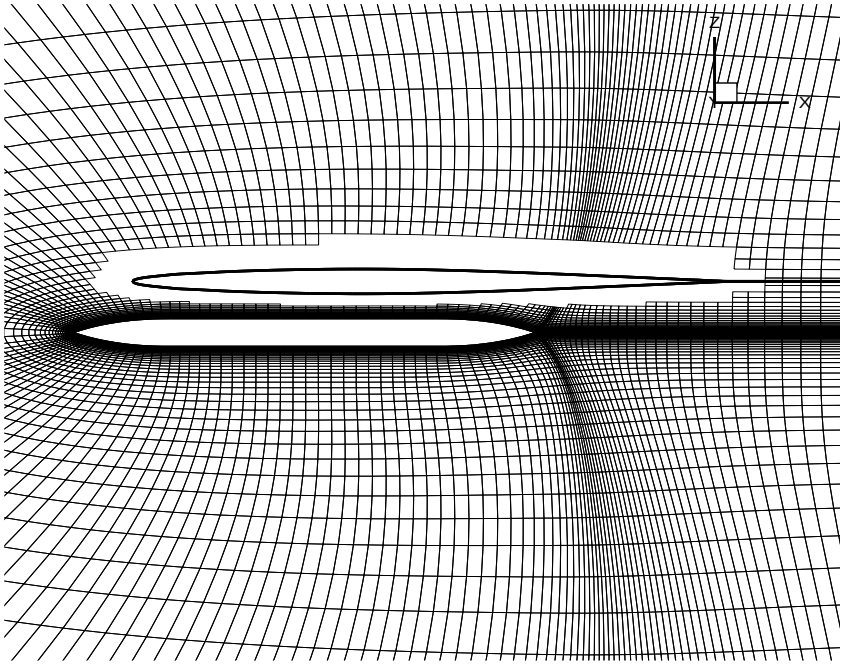

Figure 3.6.b.÷ Hole two

Biçimlendirilmiş: Sola

3.2 The Results at Different Angles of Attack

The development of a CFD capability to obtain solutions for transonic flows about this complex configuration is performed at three different angles of attack initially. The NACA64A010 airfoil and ~~OCO~~the OCO are geometrically nonsimilar and their zero degree angle-off combination is studied at different angles of attack. These prior studies of transonic flows about these components as intermediate steps are necessary to gain a better understanding of such a transonic flow around complex geometries. The angles of attack, which are considered and applied to these initial cases, are 0-degree, 2.0-degree~~,~~ and 12.0-degree. Then, different angle-off positions and different store locations are studied. Table 3.1 shows the parameters related to the cases that are studied and presented in this dissertation.

Table 3.1~~.~~: List of Cases

CASES	***AOA***	***ANGLE-OFF***	***~~OCO~~~~the~~THE OCO DISTANCE***
Case No:1	0	0	1,77d
Case No:2	2	0	1,77d
Case No:3	12	0	1,77d
Case No:4	2	0	3,0d
Case No:5	2	10	3,0d
Case No:6	2	10	6,0d

The two-dimensional cases at different angles of attack are considered to examine the effects of geometries in transonic speed regime and test the grid overlapping technique by using a composite grid. In particular~~Especially~~, the first case is chosen to make a comparison with a result in literature. ~~Also~~In addition~~Besides~~, interference flow problem of ~~OCO~~the OCO placed under NACA64A010 airfoil is also analyzed.

Transonic flow occurs when there is a mixed subsonic and supersonic local flow in the same flowfield, typically with free stream Mach numbers from 0.6 or 0.7 to 1.2. The supersonic region of the flow is usually terminated by a shock wave, allowing the flow to slow down to subsonic speeds. This complicates both computations and wind tunnel testing. However, there are some analytic theories available for guidance, especially compressible flow theory.

Biçimlendirilmiş: Yazı tipi: 12 nk
Biçimlendirilmiş: Girinti: Sol: 0 cm
Biçimlendirilmiş: Girinti: İlk satır: 0 cm
Biçimlendirilmiş: Sola, Girinti: İlk satır: 0 cm
Biçimlendirilmiş Tablo
Biçimlendirilmiş: Girinti: İlk satır: 0 cm

At some higher subsonic Mach numbers, the flow becomes sonic at a single point on the surface of the airfoils and on the surface of the stores where the flow reaches its highest speed locally. As the Mach number increases further, a region of supersonic flow develops. Normally, the flow is brought back to subsonic speed by the occurrence of a shock wave in the flow. If the free stream Mach number increases, the shock moves aft and becomes stronger. As the Mach number of the free stream approaches one, the shocks move all the way to the trailing edge. Many variations in the specific details of the flowfield development are possible, depending on the specify geometry of the airfoils and stores. This typical progression of the flow pattern leads to rapid variations in drag, lift, and pitching moment with the change in Mach number.

Accurate prediction of aerodynamic characteristics of airfoil and external store carriage is of paramount importance in transonic speed regime. In this speed regime, the interference flowfield is very critical. The interference flowfield, in which aerodynamic forces are generated by the external store, has a great influence on the flowfield of the airfoil. Furthermore, the different locations of the store and the high angle of attack are changing the influence on the flowfield and its aerodynamic relationship with the wing or the parent body. This relationship or mutual interference is mostly pronounced in the transonic speed regime.

Biçimlendirilmiş: Girinti: İlk satır: 0 cm

A finite region of supersonic flow is detected over the surfaces of individual NACA64A010 airfoil and ~~OCO~~the OCO. This supersonic region or supersonic pocket includes a strong oblique shocks at the trailing edges of the geometries. The supersonic flow has strong expansion waves propagating from the airfoil and ~~OCO~~the OCO surfaces and terminating at a place a few diameters away from the trailing edges of the geometries. The thickness of the geometries and the angle of attack cause larger perturbations in the flowfields. The flow expands to a greater degree over ~~OCO~~the OCO due to its thickness and angle of attack. The thickness of airfoil is 15% less than ~~OCO~~the OCO. Hence, transonic effects are stronger for ~~OCO~~the OCO and the local Mach numbers inside the supersonic region are greater, which in turn causes the oblique shock waves to be stronger. However, since the lift of the system is provided by the airfoil, the transonic effects on this airfoil are also very important. The Mach contours of the individual airfoil and ~~OCO~~the OCO at

0.95 Mach are shown in figures 3.7a and 3.7b respectively. ~~Besides, t~~The Cp plots of geometries are also shown in ~~the~~ figure 3.7c.

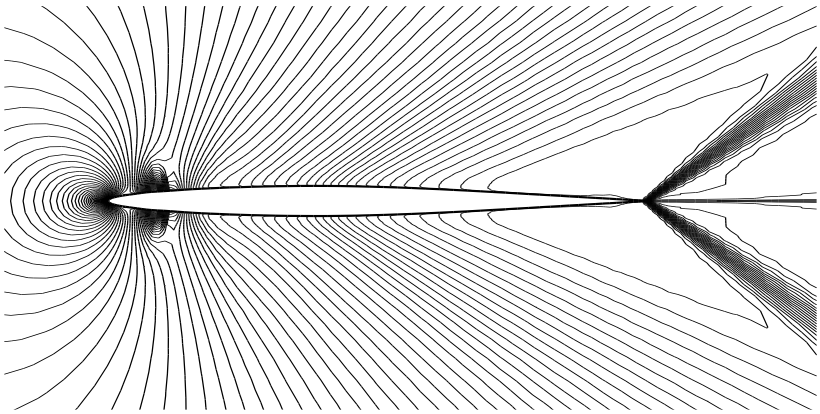

Figure 3.7.a~~:~~ Mach contours of NACA64A010 airfoil at zero AOA

Biçimlendirilmiş: Sola

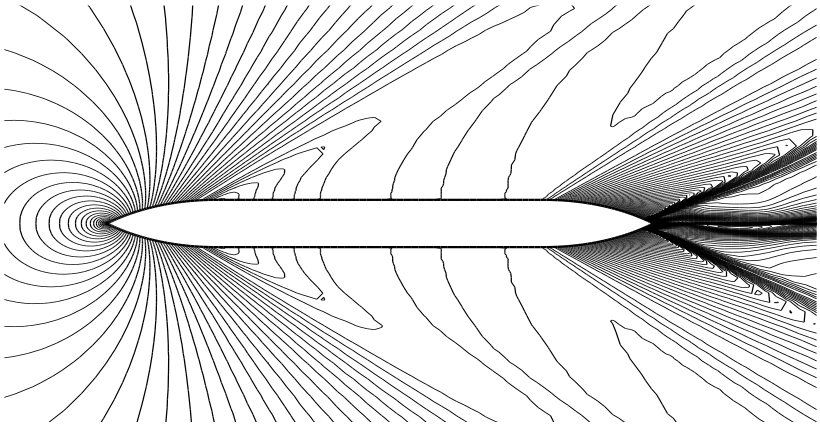

Figure 3.7.b~~:~~. Mach contours of the OCO~~ogive cylinder ogive~~ at zero AOA

Biçimlendirilmiş: Sola

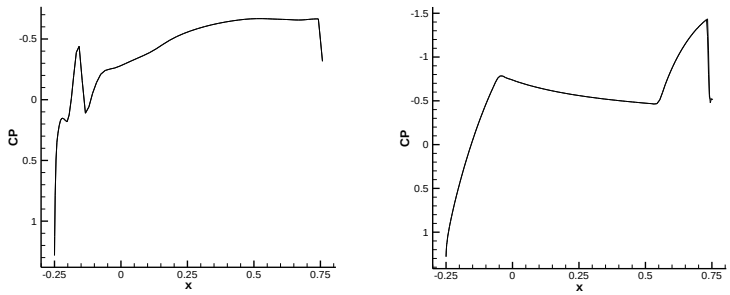

Figure 3.7 c.: Cp plots of individual airfoil and ~~OCO~~the OCO at zero AOA

Biçimlendirilmiş: Sola

When the external store is placed under the airfoil, the flow region between airfoil and store has~~gets~~ different characteristics. The flow expands isentropically from subsonic to supersonic speeds in this inbound region. In each case, at a point between airfoil and Ogive Cylinder Ogive, the sonic line is detected and the local flow Mach number continues to increase until the strong oblique shock. This sonic line is usually detected at the closest point between the airfoil and ~~OCO~~the OCO. The geometry after this sonic line has somehow expansion section characteristic and the increase in the flow speed is observed as it is expected. Due to the relative position of ~~OCO~~the OCO with respect to airfoil, the oblique shock at the trailing edge of the upper surface of ~~OCO~~the OCO is very strong that it reflects from the airfoil and merges with the oblique shock of airfoil at zero AOA. However, the local flow Mach number is still supersonic in this section. Nevertheless, after the reflected shock, subsonic local Mach numbers are also detected. This supersonic flow ended with a strong shock after the geometries and this is the boundary of the supersonic pocket. After this shock, the flow slows down to the free stream Mach number, which is 0.95. The Mach contours of this case have a strong accordance with the pressure contours and they are shown in figures 3.8a and 3.8b respectively.

Biçimlendirilmiş: Girinti: İlk satır: 0 cm

The first case chosen emphasizes the aerodynamic interference between closely spaced bodies. ~~Besides, t~~This case is chosen to make comparison with results in the literature [43, 44]. Even if the type of grids and numbers of grid points are

completely different, the results obtained at zero AOA have strong accordance with the results in the literature. The Cp distribution of this case and the result taken from the literature are presented in ~~the~~ figures 3.9a and 3.9b respectively. The bold lines in ~~the~~ figure 3.9a show the Cp distribution over the outbound surfaces of the airfoil and ~~OCO~~the OCO that~~which~~ are obtained for this case.

Since the distance between the bodies is less than one body diameter, they are mutually affecting each other's flowfields. This can be ~~clearly~~ seen clearly from the figures of contour lines and Cp distributions over inbound surfaces of airfoil and ~~OCO~~the OCO.~~.~~

Cp, which is a short form of "Pressure Coefficient," ~~,~~ is a nondimensional pressure difference ~~and it is~~ widely used in fluid dynamics. The Cp plot can be used to understand the pressure changes and the other pressure dependent variables over the airfoil and external store.

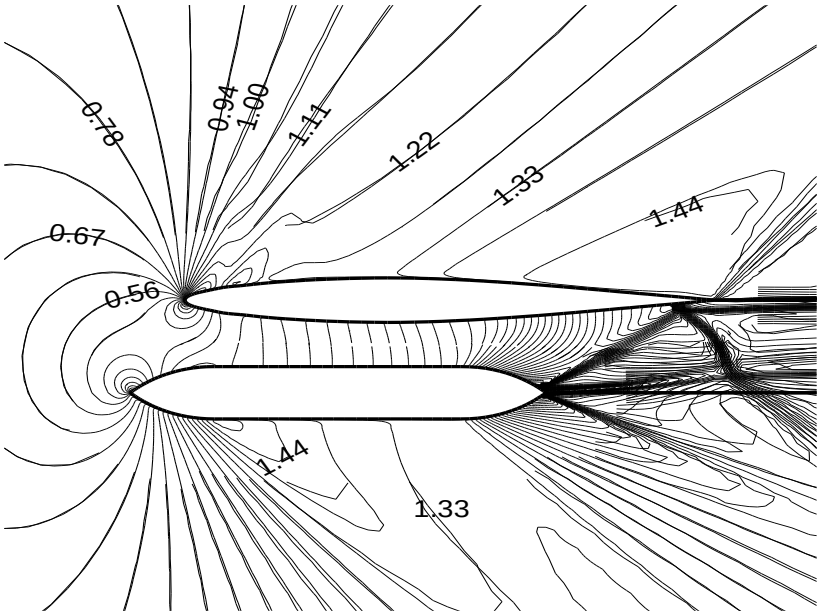

Figure 3.8.a.~~:~~ Mach contours at zero AOA

Biçimlendirilmiş: Sola

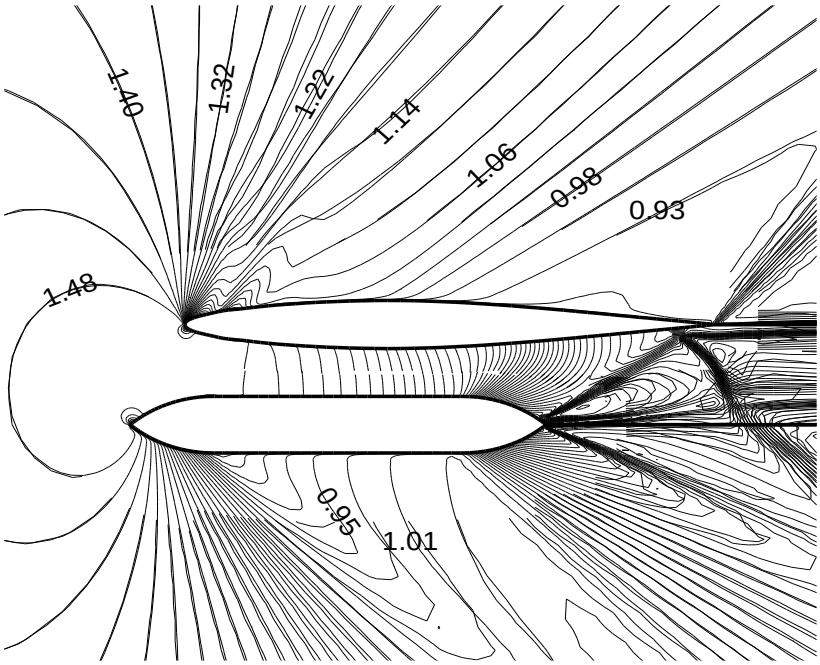

Figure 3.8.b.: Pressure contours at zero AOA

Biçimlendirilmiş: Sola

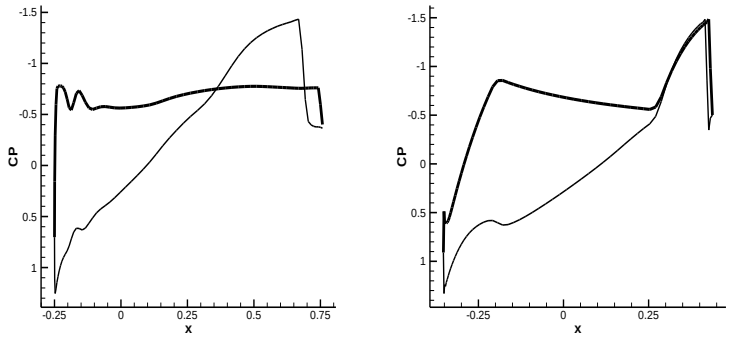

Figure 3.9.a.: Cp plots of NACA64A010 airfoil and ~~OCO~~the OCO at zero AOA

Biçimlendirilmiş: Sola

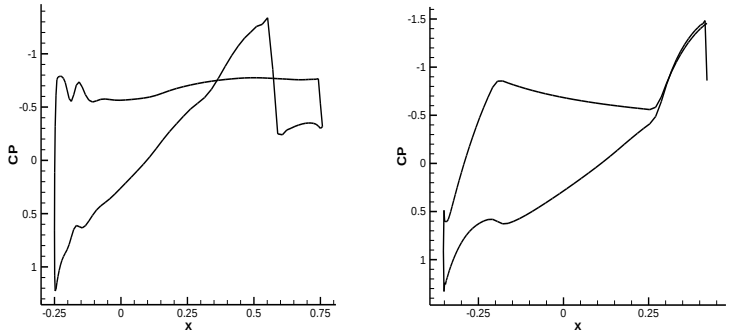

Figure 3.9.b.: Cp plots of NACA64A010 and ~~OCO~~the OCO at zero AOA [43, 44]

Biçimlendirilmiş: Sola

Biçimlendirilmiş: Girinti: İlk satır: 0 cm

The continuous increase shows that the flow accelerates continuously in the shock pocket and it ends with a sharp decrease in the Cp plot. The sharp pressure change or jump observed in a Cp plot shows that a strong shock exists over the outbound surfaces of the airfoil and ~~OCO~~the OCO. In order to compare the results, the flow around NACA64A010 airfoil and ~~OCO~~the OCO are solved individually in the same flow conditions and in the same flow solver. These independent results have shown that the Cp distributions of the NACA64A010 airfoil and ~~OCO~~the OCO outbound

surfaces, which are shown in figure 3.7c, have almost similar characteristics with the results obtained from the combination of these two geometries in figure 3.9a. However, the inbound surfaces of these geometries have different pressure distributions as they are compared with the individual results, which are show in the same figure.

The Cp distributions of the upper surface of the airfoil are slightly different from the independent results obtained for the same airfoil. The similar Cp difference is also valid for lower part of the ~~OCO~~~~the~~ OCO. The main reason behind this slight difference is the interference flow. Due to the relative position of the bodies, interference flow is not only affecting the flow over the inbound surfaces but also the outbound surfaces of the bodies. Moreover, the use of overlapped grids is also another reason ~~of~~for this slight difference. Despite the each body use its own grid in the hole, due to the interpolation procedure from the other grid may cause such slight differences in the results. However, if they are compared to the independent results of these bodies, the Cp distributions of the inbound surfaces of the airfoil and ~~OCO~~the OCO are completely different. This is one of the main indications of the interference flowfield of complex geometries. The shocks can be apparently seen in the interference flowfield and the harmony of Cp plots with the Mach or pressure contours is exactly approving the precise locations of the shocks. Note that the shock wave on the lower part of the airfoil is caused by the reflecting shock from the ~~OCO~~~~the~~ OCO in the first case.

The computational rate of the first case with complex geometries by mesh sequence is 38.10 microseconds per cell per iteration. The iteration number for this case is twenty thousand and the complete run lasted for this steady state solution is four hours, twenty-four minutes and twelve seconds. For the independent solutions of NACA64A010 airfoil and ~~OCO~~the OCO, the computational rates are 30.89 and 36.15 microseconds per cell per iteration respectively. The total CPU time is 8046.11 seconds for ogive cylinder ogive, and 3856 seconds for NACA airfoil.

The second and third cases have chosen ~~at~~ 2.0 and ~~12.0 degree~~12.0-degree~~s~~ angles of attack to investigate and emphasize the effects of higher angle of attack to the interference flowfield between closely spaced bodies. The frontal and downward distances and the angular position of the bodies remain the same for these cases. The shock pocket occurred in these cases has relatively different characteristic and

Biçimlendirilmiş: Girinti: İlk satır: 0 cm

location due to the higher AOA. Especially for the third case, the shock pocket over outbound surface of the wing has greater local Mach numbers than the second case. However, the shock pocket over the outbound surface of ~~OCO~~the OCO in the third case is weaker than the second case. The location of this shock pocket is also very far behind its half part.

At a point between the airfoil and ogive cylinder ogive, the sonic line is also detected and the local flow Mach number continues to increase in these cases. However, the local Mach numbers of the third case are less than the ones~~e~~ in ~~of~~ the second case. As the numerical values are compared for the interference flowfield, there is approximately a 12% difference between the local Mach numbers in the second and third cases. The frontal location of the external store is the main reason of this difference because the frontal location of the external store affects the incoming flow characteristics of the region between the geometries. The Mach contours of cases two and three are shown in figures 3.10 and 3.11 respectively. It can be said that the characteristics of flowfield and location of the shock are slightly different. For the third case, the oblique shock at the trailing edge of ~~OCO~~the OCO reflects from the airfoil without merging and makes the oblique shock of the airfoil disappeared at the trailing edge. Cp plots of this flow have a strong accordance with the Mach contours and they are shown in figures 3.12a and 3.12b. It should be noted that the bold lines show the Cp distributions of the outbound surfaces of the bodies.

The computational rate of the second and third cases with complex geometries by mesh sequence is 49.87 and 49.23 microsecond per cell per iteration respectively. The iteration number for these cases is again twenty thousand and the convergence histories of these cases are shown in the figure 3.12c.

The initial results show that there is a strong aerodynamic interference between closely spaced bodies. Since the distance between the centerlines of the bodies is 1.77 diameters and their angle-off is zero degree, they ~~are~~ mutually affect~~ing~~ each other's flowfields. As the AOA increases, the general characteristics of this complex flowfield remain the same but some remarkable changes in this interference flowfield are detected.

In the next chapter, the results at different store locations and different angle-off positions between the bodies are investigated. The AOA is chosen 2.0 for the rest of

the cases in order to show the aerodynamic interference of the bodies at different store locations and angle-off positions at 0.95 Mach.

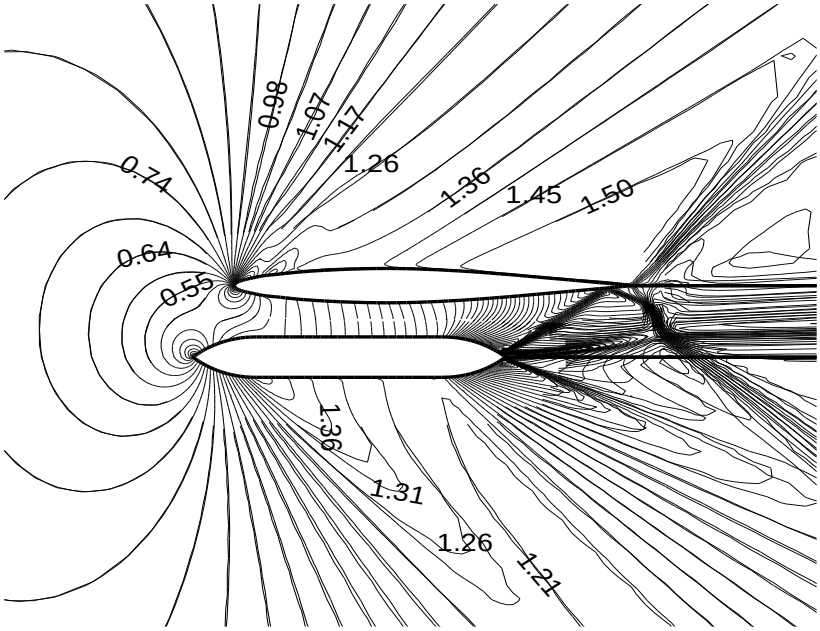

Figure 3.10.÷ Mach contours at 2.0 AOA

Biçimlendirilmiş: Sola

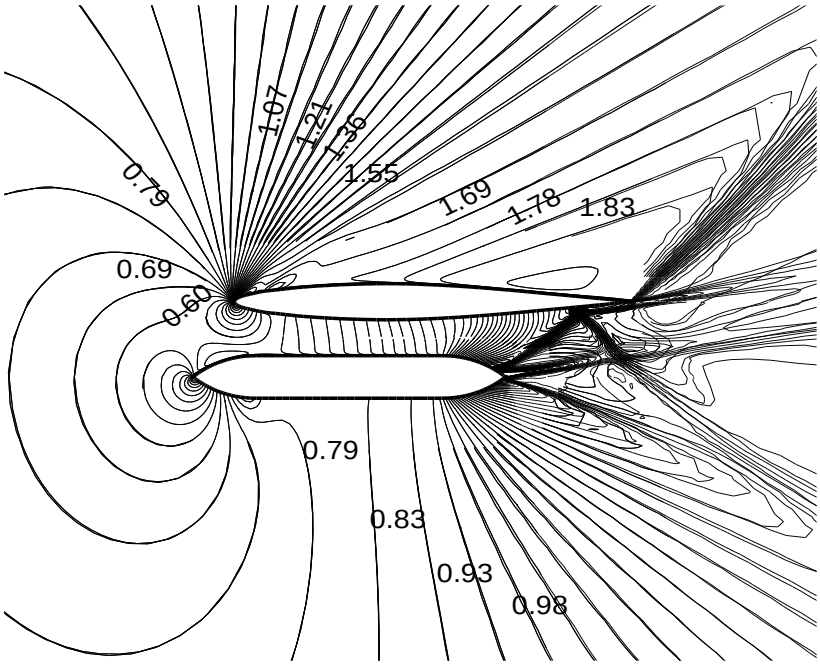

Figure 3.11.: Mach contours at 12 AOA

Biçimlendirilmiş: Sola

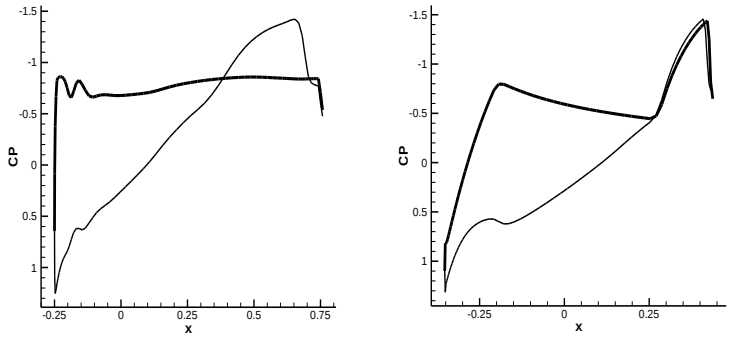

Figure 3.12.a.÷ Cp plots of NACA64A010 airfoil and ~~OCO~~the OCO at 2.0 AOA

Biçimlendirilmiş: Sola

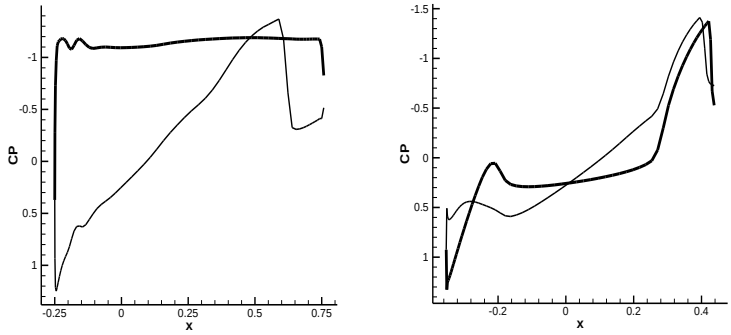

Figure 3.12.b.÷ Cp plots of NACA64A010 airfoil and ~~OCO~~the OCO at 12 AOA

Biçimlendirilmiş: Sola

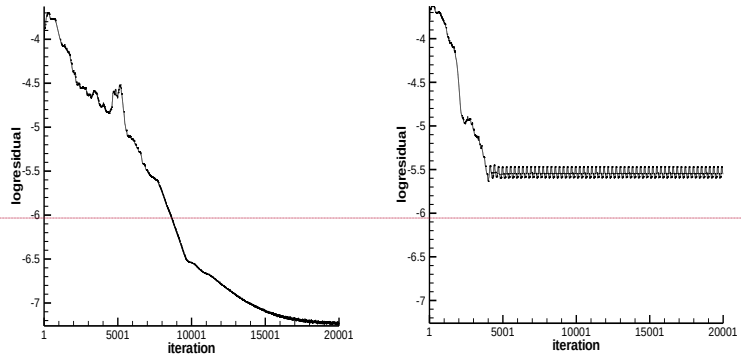

Figure 3.12.c.÷ Convergence history of ~~c~~Case ~~two~~2 & ~~three~~3

Biçimlendirilmiş: Sola

3.3

Biçimlendirilmiş: Yazı tipi: 12 nk

Biçimlendirilmiş: Girinti: Sol: 0 cm

The nd

Biçimlendirilmiş: Girinti: İlk satır: 0 cm

ang he

gird ce

between the bodies and angular position of the external store with respect to airfoil.

In the fourth case, the only changed parameter is the distance between the airfoil and ~~OCO~~the OCO as it is compared to initial cases, which are three diameters. The angle off is zero degrees for this case. The fifth case is chosen so that~~,~~ the distance between the geometries~~bodies~~ remains three diameters but the angle off is chosen ten degrees nose down position of ~~OCO~~the OCO. Finally, for the sixth case, the angle off position of ~~OCO~~the OCO, which is ten degrees, remained the same ~~as it is~~ compared to the fifth case, but the distance between the bodies ~~is~~ increased to six diameters. Moreover, the free stream Mach number is 0.95 and the angle of attack is 2.0 degrees for all of the cases. Table 3.1 in the previous chapter~~,~~ shows the parameters related to the cases.

The program MaGGiE is executed again for each of the cases mentioned in this chapter~~,~~ because the relative position of the ~~OCO~~~~the~~ OCO and its grid with respect to NACA64A010 airfoil have been changed. MaGGiE determines the stencils for the fringe points of grid one and grid two again. For the fourth and fifth cases, the fringe points of grid one, which are interpolated from grid two, are 141 and 148 respectively. Similarly, the fringe points of grid two, which are interpolated from grid one, are 265 and 267 respectively. For the last case, there are 112 fringe points of grid one, which are interpolated from grid two and there are 248 fringe points of grid two, which are interpolated from grid one. As the store moved away from airfoil, the overlapped region is getting smaller and the number of fringe points is decreasing.

In the same way, no boundary conditions are applied to the outer boundary of grid two and these outer points are used for interpolation from grid one. The total number of boundary points of grid two for which stencils must be determined is 576. The total number of boundary points is the same for all of the cases~~,~~ because the dimensions and the total number of the grid points are not changed. The total number of cells is 20800 and the total number of grid points is 42636.

The steady state results are obtained for these cases in the same way mentioned in the previous chapter. Since the distance and angular position of the ~~OCO~~ OCO are changed, the bodies are still mutually affecting each other's flowfields. A finite region of supersonic flow is again detected over the surfaces of NACA64A010 airfoil and ~~OCO~~the OCO in each case. In this supersonic region, strong oblique shocks exist at the trailing edges of the bodies but they have different characteristics

in these cases. Mach contours of these cases are shown in ~~the~~ figures 3.13, 3.14 and 3.15. The harmony of the shocks can be apparently seen in the Mach contour figures and Cp plots. In other words, Cp plots are exactly approving the precise locations of the shocks in the Mach contour figures. The Cp plots of these cases are shown separately for the airfoil and ~~OCO~~the OCO in ~~the~~ figures 3.16a, 3.16b and 3.16c. The bold lines show the Cp distributions of outbound surfaces of airfoil and ~~OCO~~the OCO in the figures.

At the some points in the flow region between the airfoil and ~~OCO~~the OCO, the sonic line is also detected but the sonic line between the bodies is closer to the trailing edges in these cases because the increase in the distances of the bodies changes the incoming flow properties for this interference flowfield. Moreover, the frontal location of ~~OCO~~the OCO in the fourth case still affects the incoming flow between the bodies. The local flow Mach number continues to increase until the strong oblique shocks. As it is expected, the increase in the distance also affects the local Mach numbers. The maximum local Mach numbers are not as much as the initial cases. Furthermore, the oblique shock at the trailing edge of the store does not reflect from the lower surface of the airfoil because the bodies are not closely spaced anymore. It can be said that as the store moved away from the airfoil, the interference flowfield changes characteristic. Moreover, the ten-degree nose down angle of ~~OCO~~the OCO in the fifth and sixth cases increases the pressure between the bodies.

Especially for the last case, as the distance is increased to 6.0 diameters, the intersection of the oblique shocks can be seen in the interference flowfield instead of reflecting or merging. It means that mutual interaction of the bodies is decreasing gradually as the distance is increased but not completely. The determination of the distance that bodies do not affect each other's flowfield can be found by solving a store separation problem in which these steady state results are used as the initial cases.

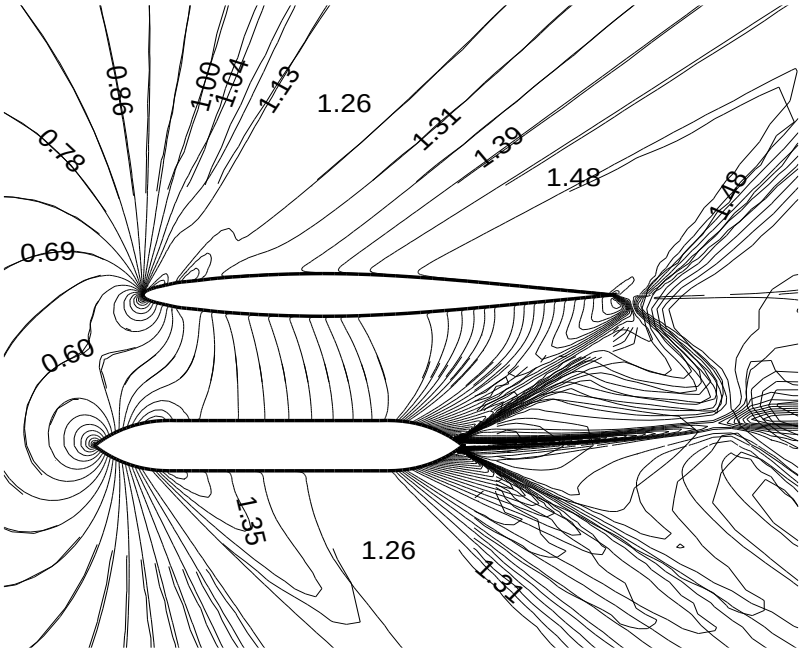

Figure 3.13.÷ Mach contours of case four4 at 2.0 AOA

Biçimlendirilmiş: Sola

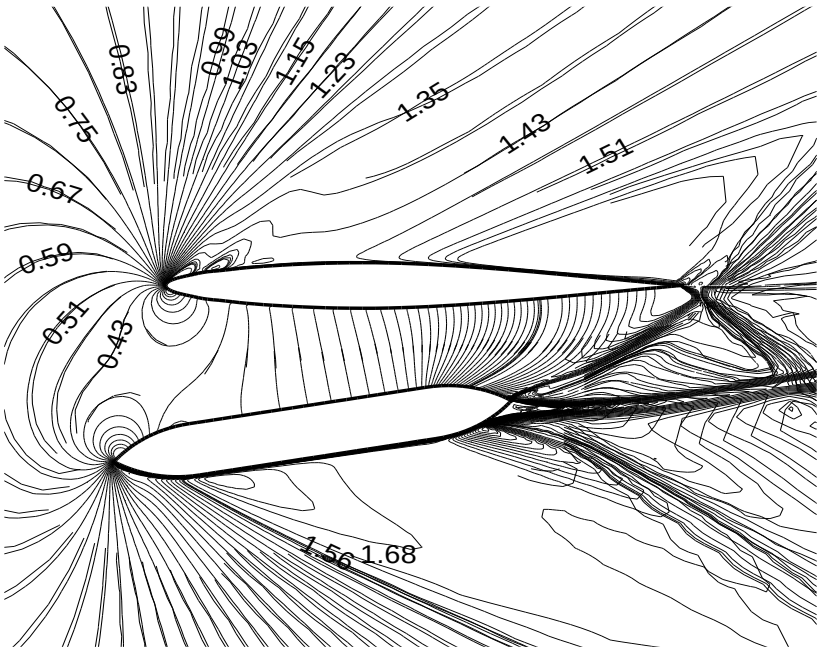

Figure 3.14÷. Mach contours of case five5 at 2.0 AOA

Biçimlendirilmiş: Sola

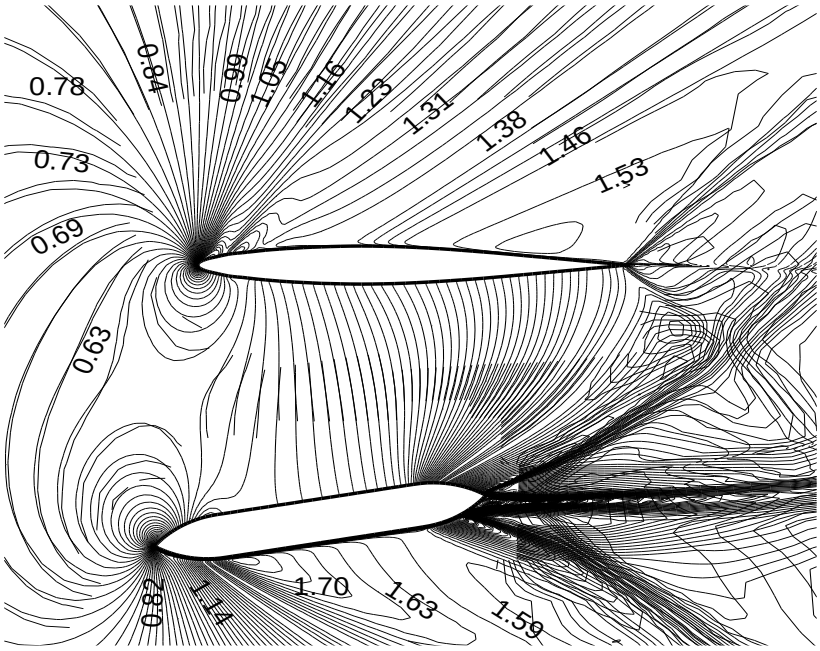

Figure 3.15.~~:~~ Mach contours of case six~~6~~ at 2.0 AOA

Biçimlendirilmiş: Sola

The computational rate of the fourth and fifth cases with complex geometries by mesh sequence is 43.81 and 43.61 microseconds per cell per iteration respectively. The computational rate of the last case is 36.88 microseconds per cell per iteration. The iteration number for these cases is also twenty thousand and the convergence histories of these cases are shown in ~~the~~ figures 3.17a, 3.17b and 3.17c.

Biçimlendirilmiş: Girinti: İlk satır: 0 cm

Although the distance between the bodies is changed, these results show that there is still a strong aerodynamic interference between flowfields of the bodies. This interaction of the bodies affects each other's aerodynamic characteristics. Since the distance between the bodies is increased to 3.0 or 6.0 diameters and their angle-off is ten degrees, they ~~are~~ mutually affect~~ing~~ each other's flowfields.

It should be noted that the discontinuous Mach contours of these last cases across the overlapped region could be observed. This problem is more pronounced if the cell centers of different subdomain grids in the overlapped region are further away from each other. It can be said that as the store is moved away from the airfoil, the capability of interpolating data across the overlapped region is not as good as the initial closely spaced bodies' cases.

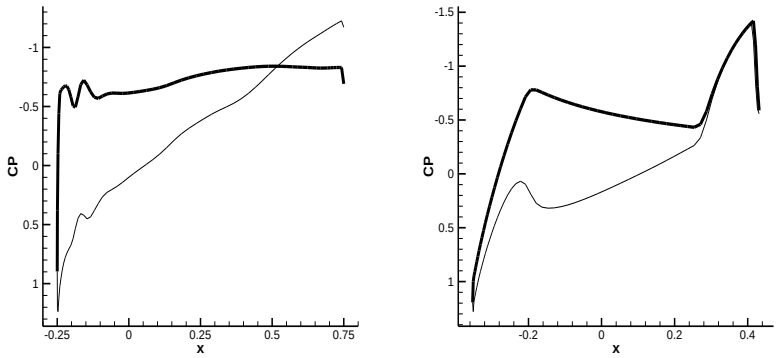

Figure 3.16.a.÷ Cp plots of NACA64A010 airfoil and ~~OCO~~the OCO ~~at 2.0 AOA~~ (Case ~~four~~4)

Biçimlendirilmiş: Sola

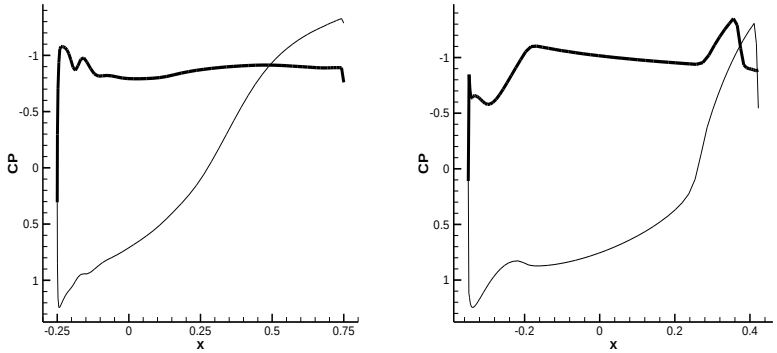

Figure 3.16.b.÷ Cp plots of NACA64A010 airfoil and ~~OCO~~the OCO ~~at 2.0 AOA~~ (Case ~~five~~5)

Biçimlendirilmiş: Sola

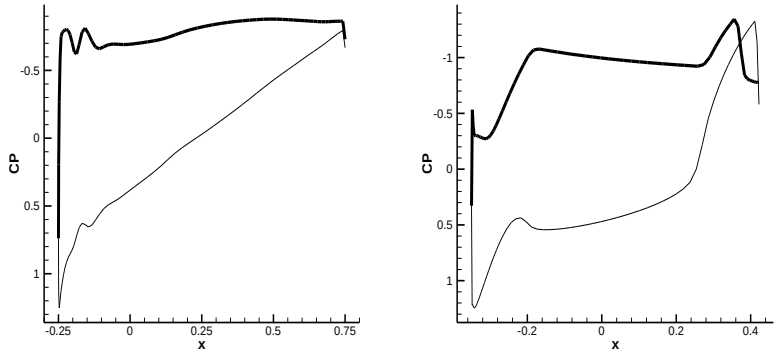

Figure 3.16.c.÷ Cp plots of NACA64A010 airfoil and ~~OCO~~the OCO ~~at 2.0 AOA~~ (Case ~~six~~6)

Biçimlendirilmiş: Sola

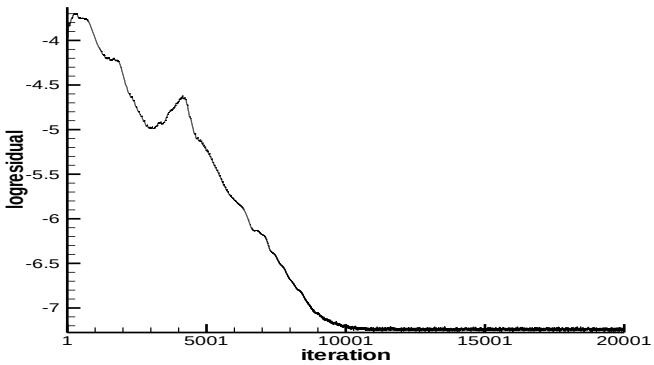

Figure 3.17.a.: Convergence history of case four

Biçimlendirilmiş: Sola

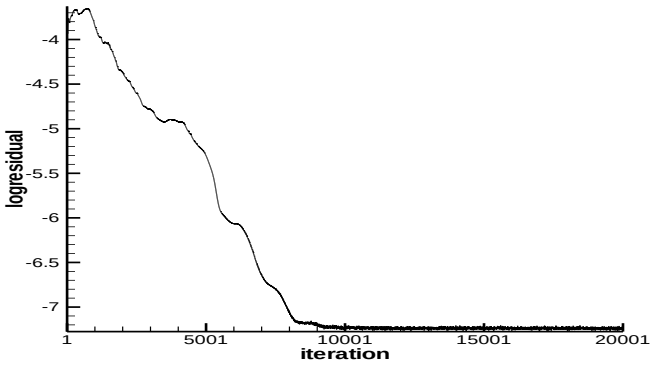

Figure 3.17.b.: Convergence history of case five

Biçimlendirilmiş: Sola

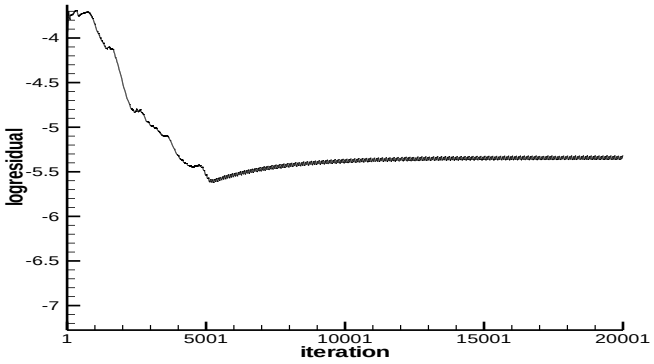

Figure 3.17.c.: Convergence history of case six

Biçimlendirilmiş: Sola

In the he

Biçimlendirilmiş: Girinti: İlk satır: 0 cm

method nd

momen al

results. or

the cor te

Suggestions for the further investigations about the subject also are also presented.

4. CONCLUSIONS AND RECOMMENDATIONS

A numerical algorithm that accurately simulates and solves complex flow problems must be used with regard to the types of geometries and characteristics of flows being considered. The algorithm must possess the ability and the flexibility to consider any arbitrary complex configurations without further burden on available computer resources. The governing equations being solved, the discretization and the difference methods of these equations are also essential elements of the solution algorithm. Efficiency of the algorithm is another desirable feature that must be addressed. A finite volume solver for the structured grids, which was developed in the early 1980's and is called CFL3D, has all of these features and used as a numerical algorithm in this study.

For many of the configurations studied earlier, solving the Euler equations or the full potential equations is sufficient for design purposes. However, for detailed analysis of a flow where diffusion effects are not negligible, the use of Navier Stokes equations is required. The Euler equations are often used to study compressible flows at high Mach numbers. At high velocities, the Reynolds number is very high and viscous and turbulence effects are important only in a small region near the walls. For this reason, Euler equations can be used when the viscous effects are small and the inviscid flow includes strong shock waves [45]. Since the main objective of this present work is to investigate the interference flow around complex configurations, the solutions of Euler equations are sufficient for reaching some reasonable results. In this study, the Euler equations are solved by using an implicit, upwind biased, finite volume method.

Inviscid flows, where various types of shocks may exist in the flow domain, make up a large portion of the recent CFD research. The implicit scheme eases the restriction on the time step for highly stretched grids. The upwind method of flux difference splitting of Roe, which is used for the inviscid Euler equations, is useful in obtaining crisper resolution of the high flow gradients, such as shocks. Additionally, it has the advantage of being naturally dissipative; hence, separate spatial dissipation terms are

not used to overcome oscillations or instabilities arising in regions of high gradients. It is also beneficial to discretize Euler equations using a finite volume method. The finite volume formulation begins with the integral equations and satisfies the integral conservation laws. Thus, it remains valid in the presence of large gradients in the flowfield and satisfies the conservation laws. It should be noted that the finite volume discretization allows more flexibility with regard to the geometry and it is tolerant of grid singularities.

A domain decomposition method called grid overlapping is used to investigate interference flow around complex configurations in this study. The domain decomposition method increases the flexibility of grid generation for complex configurations and in turn enhances the ability to simulate and analyze the flowfield with complicated features. For example, domain decomposition methods make it possible to solve the flow around various shapes and models can be considered for the store and the parent body. Furthermore, the simplicity of grid generation with domain decomposition techniques allows representing the critical regions of a flowfield with very fine meshes. This subsequently increases the computational time required to obtain the solution on these meshes. The largest contribution of the DDT may be the possibility of analyzing and understanding the interference flowfield that exists between multiple complex configurations. This is very important since these types of flows pose enormous challenges for experimental techniques. For example, Schlieren photographs are not always available and vapor screen photographs are limited in providing information.

Grid overlapping, also known as the overset grid or CHIMERA technique, requires neither one-to-one connectivity nor a shared interface to pass flow information from one grid to another. The construction of the overlapped grids for the present study is accomplished by the MaGGiE code. MaGGiE code is used to create the two-dimensional composite grids from individual subdomain “C type” grids. It also provides the necessary information for the intergrid communication. The subdomain grids create holes in each other in which they are overlapped. The main idea behind the holes is that the grid points, which belong to base grid, are excluded from the solution of the subdomain grid. It can be said that MaGGiE code, the composite grid generator, is very suitable for CFL3D and effectively used.

The geometry, free stream conditions and Mach contours of the airfoil and store are presented in the previous chapter. The geometry of the airfoil is NACA64A010 and the store is idealized as an ogive-cylinder-ogive store in carriage position several diameters away from the airfoil. The free stream Mach number 0.95 from the front and temperature 460 R are applied to this airfoil and store assembly. The composite grid of cases consists of two grids: A smaller C type grid wrapped around the store and overlapped on a C type grid generated for the airfoil.

In the results, a finite region of supersonic flow is detected on the surfaces of NACA64A010 and the Ogive Cylinder Ogive. This embedded supersonic region, namely the supersonic pocket, includes strong oblique shocks at the trailing edges of the geometries. The supersonic flow has strong expansion waves propagating from the airfoil and Ogive Cylinder Ogive's surfaces and terminating at the sonic line at back of the geometries. Note that as the thickness of the airfoil and store causes a larger perturbation of the flow, the flow expands to a greater degree over a thicker body. Hence, transonic effects are stronger for thicker bodies. The local Mach numbers inside the supersonic region become larger, which in turn causes the terminating shock waves to be stronger.

The contour lines of cases are shown in the previous chapter. The discontinuous contour lines across the overlapped grids can be observed. This problem is more pronounced if the cell centers of different subdomain grids in the overlapped region are further away from each other. The main reason behind this problem is the number of grid connections in the overlapped regions. An overlapped region of five to ten cells is found to be adequate for proper grid connections without redundant information being passed between subdomain grids. It should be noted that all of the contour figures in this dissertation are generated by TECPLOT 7.5 [46], which is not capable of interpolating data across the overlapped boundary.

The steady state Cp distributions on the airfoil and the Ogive Cylinder Ogive are presented and the harmony of Cp plots, and Mach or pressure contours are exactly approving the precise locations of the shocks. The bold lines in the Cp plots are drawn to show the outbound surfaces' Cp distributions. The pressure difference between the upper and lower at different store location cases are much smaller than it was in the closely spaced position, which can be attributed to two reasons. The first reason is the elevated lower surface pressures due to pitching down of the store

and the second is the widening gap between the store and wing that reduces the interference effects. As a result, the results show that CFL3D is capable of analyzing proposed problems.

In order to understand the interference flow around complex geometries, the change in lift, drag and moment coefficients should also be discussed. The numerical results for lift-drag and moment coefficients of the cases are presented in table 4.1. In order to make a comparison, individual single airfoil results are also presented. If the pitching moment is in counter-clockwise or pitch up direction, the moment coefficient is positive.

Since the airfoil is axisymmetric, the lift and moment coefficient of single airfoil at zero AOA is zero. However, after the store is placed under airfoil due to changing pressure between the bodies, the lift, drag and moment coefficients are increasing. In addition, an increase in AOA and distances between bodies also increases the lift and drag coefficients of the complex geometry. However, after the store is placed under airfoil at 12 AOA case, the lift, drag and moment coefficients are decreasing. The frontal location of the store and high AOA change incoming flow characteristics and cause an inevitable decrease in pressure between the bodies. The location of the store and the change in AOA also affects pitching moment. For stability conditions, negative pitching moment is always required. Moreover, the location of the store is dependent to center of gravity of the system.

Table 4.1. List of Lift, Drag, and Moment Coefficients

CASES	***AOA***	C_L	C_D	C_{MY}
Single Wing	0	0,0000	0,0791	0,0000
Single Wing	2	0,2248	0,0853	-0,0363
Single Wing	12	1,2104	0,3111	-0,2602
Case No:1	0	0,3275	0,0964	0,0882
Case No:2	2	0,3945	0,1127	0,0857
Case No:3	12	0,8318	0,2651	-0,0701
Case No:4	2	0,3949	0,1024	0,0356
Case No:5	2	0,8047	0,1196	0,0324
Case No:6	2	0,7830	0,1008	-0,0778

The iteration number for all of the cases is twenty thousand, and the convergence histories of these cases are presented in the previous chapter. The computation rate and total run time for the complex geometry and single airfoil cases are presented in table 4.2. The computation rate and the total run time of the individual single airfoil cases are apparently lower than complex geometry cases. As the store is moved away from the airfoil, the overlapped region is being reduced. It means that if the bodies are being closely spaced and the angle of attack is increased, the problem is getting more and more difficult and requires more computation time. The complexity of the cases can be easily understood by comparing the computation rates and total run times that are presented in table 4.2.

Table 4.2. Computational Times of Cases

CASES	***COMPUTATION RATE*** (microseconds/cell/iteration)	***TOTAL RUN TIME***
Single Wing (0 AOA)	30.89	1h. 04min. 16sec.
Single Wing (2 AOA)	39.78	1h. 22min. 46sec.
Single Wing (12 AOA)	30.63	1h. 03min. 44sec.
Case No:1	38.10	4h. 24min. 12sec.
Case No:2	49.87	5h. 46min. 08sec.
Case No:3	49.23	5h. 41min. 23sec.
Case No:4	43.81	5h. 03min. 47sec.
Case No:5	43.61	5h. 02min. 41sec.
Case No:6	36.88	4h. 15min. 45sec.

Results seem reasonable; however, they are two-dimensional, which does not allow the lateral relieving effect of axisymmetric or three-dimensional flows. In other words, three-dimensional solutions add relieving effect to the two-dimensional results. However, these two-dimensional results are sufficient for understanding the interference flow around complex geometries, and they can be used in unsteady store separation problems as the initial cases. Moreover, there is no experimental data to validate these computational results, but the first case is chosen to make comparison with results in the literature. Nevertheless, there is no single method that has been verified for a complete range of complex geometry problems and development and verification of CFD methods always require experimental data.

After reviewing the relevant literature, it is apparent that the interference flows have not been studied extensively. These investigations generally bear very restrictive assumptions. Hence, there appears to be an urgent need for further and more comprehensive investigations, using both experimental and computational methods. In particular, interference flows encountered in external store carriage, multi store carriage and especially stores with fin or canard and their separation from the parent body have not been computationally investigated extensively.

As new stores are put in service or investigations of aircraft and new store compatibility will continue to be important since existing aircraft remain in service for along time. One of the most important problems associated with store carriage is the safe separation of stores from a pylon or weapon bays of aircraft. The release of stores from maneuvering aircraft with additional chances of physical interference also remains important phenomenon for future investigation. In the future, new aircraft/store configurations, super maneuvering aircraft, unconventional store shapes and store separation at hypersonic speeds will offer new challenges.

REFERENCES

[1] **Wood, M. F. E.,** 1989. Application of Experimental Techniques to Store Release Problems, Proceedings; NEAR Conference on Missiles Aerodinamics, Nielsen Engineering& Research, Mountain View, CA, pp 5/1-44.

[2] **Arnold, R. J. and Epstein, C. S.,** 1986. Store separation Flight Tests, AGARD AG-300, Vol. 5.

[3] **Hemsch, M. J.,** 1991. Tactical Missile Aerodynamics: General Topics, Lockheed Engineering& Sciences Company, VA, pp 578-581.

[4] **Fouladi, K.,** August 1990. Navier-Stokes Simulations of Flows About Complex Configurations Using Domain Decomposition Techniques, Ph. D. Dissertation, Mechanical Engineering Department, ODU.

[5] **Atta, E.,** January 1981. Component Adaptive Grid Interfacing, AIAA-81-0382.

[6] **Atta, E. and Vadyak, J.,** June 1982. A Grid Interfacing Zonal Algorithm for Three Dimensional Transonic Flows about Aircrafts Configurations, AIAA-82-1017.

[7] **Steger, J. L., Dougherty, F. C., and Benek, J. A.,** June 1983. A Chimera Grid Scheme, ASME Symposium on Advances in Grid Generation, FED-Vol. 5, Huston, Texas.

[8] **Benek, J. A., Steger, J., L., and Dougherty, F. C.,** July 1983. A Flexible Grid Embedding Technique with Application, AIAA-83-1944.

[9] **Benek, J. A., Donegan, T. L., and Sush, N. E.,** June 1987. Extended Chimera Grid Embedding Scheme with Application to Viscous Flows, AIAA-87-1126.

[10] **Benek, J. A., Steager, J. L., Dougherty, F. C., and Buning, P., G.,** April 1986. Chimera: A Grid Embedding Technique, AEDC-TR-85-64, Arnold Engineering Development Center Report.

[11] **Dougherty, F. C., Benek, A. J., and Steager, J. L.,** October 1985. On Applications of Chimera Grid Scheme to Store Separation, NASA-TM-88193.

[12] **Dougherty, F. C. and Kuan, J. H.,** January 1989. Transonic Store Separation Using a Three-Dimensional Chimera Grid Scheme, AIAA-89-0637-CP

[13] **Fox, J. H. and Allee, E. G.,** June 1989. Experimental/Computational Study of a Transonic Aircraft with Stores, AIAA-89-1932.

[14] **Meakin, R. L. and Suhs, N. E.,** June 1989. Unsteady Aerodynamic Simulation of Multiple Bodies in Relative Motion, AIAA-89-1996-CP.

[15] **Chow, R. and Marconi, F.,** January 1989. A Navier Stokes Solution to Hypersonic Store Separation Flow Fields, AIAA-89-0031.

[16] **Lohner, R.,** July 1988. Adaptive Remeshing for Transient Problems with Moving Bodies, AIAA-88-3736CP.

[17] **Chesshire, G. and Henshaw, W. D.,** November 1987. Multigrid on Composite Meshes, SIAM Journal Scientific Statistical Computing, Vol. 8, No. 6, pp. 914-923.

[18] **Chesshire, G. and Henshaw, W. D.,** January 1989. Composite Overlapping Meshes for the Solution of Partial Differential Equations, IBM Research Report, RC 14355.

[19] **Baysal, O., Fouladi, K., and Lessard, V. R.,** March 1989. A Multigrid Domain Decomposition Scheme with Embedded/Overlapped and Zonal Grids, SIAM Conference on Domain Decomposition Methods, Huston, TX.

[20] **Baysal, O. and Lessard, V. R.,** February 1990. An Overlapped Grid Method for Multigrid Finite Volume/Difference Flow Solvers, NASA-CR- 182008, NASA LaRC, Hampton, VA.

[21] **Baysal, O., Fouladi, K. and Lessard, V. R.,** April 1991. A Multigrid and Upwind Viscous Flow Solver on Three-dimensional Overlapped and Embedded Grids, AIAA-89-0464.

[22] **Lessard, V. R.,** December 1989. Domain Decomposition for Multigrid, Finite Volume Flow Solvers, Master Thesis, Mechanical Engineering and Mechanics Department, Old Dominion University, Norfolk, VA., USA.

[23] **Thompson, J. F.,** March 1988. A Composite Grid Generation Code for General Three Dimensional Regions – The EAGLE Code, AIAA Journal, Vol. 26, No. 3, p 271.

[24] **Belk, D. M. and Whitfield, D. L.,** January 1987. Three Dimensional Euler Solutions on Blocked Grids Using an Implicit, Two-Pass Algorithm. AIAA-87-0450.

[25] **Lijewski, L. E.,** May 1986. Transonic Flow Solutions on a Blunt Finned Body of Revolution Using the Euler Equations, AIAA-86-1082.

[26] **Lijewski, L. E.,** August 1987. Transonic Flow Solutions on a Blunt, Body-Wing-Canard Configurations Using the Euler Equations, AIAA-87-2273.

[27] **Lijewski, L. E.,** January 1989. Transonic Euler Solutions on Mutually Interfering Finned Bodies, AIAA-89-0264.

[28] **Cottrell, C. J., Martinez, A. and Chapman, G. T.,** January 1987. A Study of Multi-Body Aerodynamic Interference at Transonic Mach Numbers, AIAA-87-0519.

[29] **Cottrell, C. J. and Lijewski, L. E.,** September 1988. Finned Multi-Body Aerodynamic Interference at Transonic Mach Numbers, Journal of Aircraft, Vol. 25. No. 9, pp.827-834.

[30] **Arabshahi, A. and Whitfield, D. L.,** August 1989. A Multi-Block Approach to Solve the Three Dimensional Unsteady Euler Equations About a Wing-Pylon-Store Configuration, AIAA-89-3401.

[31] **Dietz, W. E. and Suhs, N. E.,** August 1989. Pegsus 3.0 User's Manual, AEDC-TR-89-7.

[32] **Jameson, A., Schmidt, W., and Turkel, E.,** June 1981. Numerical Solution of the Euler Equations by Finite Volume Methods Using Runge-Kutta Time Stepping Scheme, AIAA-81-1259.

[33] **Anderson, W. K., Thomas, J. L., and Van Leer, B.,** September 1986. Comparison of Finite Volume Flux Vector Splitting for the Euler Equations, AIAA Journal, Vol 24, No.9.

[34] **Roe, P.L.,** 1981. Approximate Riemann Solvers, Parameter Vectors and Difference Schemes, Journal of Computational Physics, Vol. 43, No. 2, 357-372.

[35] **Thomas, J. L., Van Leer, B., and Walters, R. W.,** June 1990. Implicit Flux-Split Schemes for the Euler Equations, AIAA Journal, Vol. 28, 973-974.

[36] **Anderson, W. K., Thomas, J. L., and Whitfield, D.L.,** 1988. Three-Dimensional Multigrid Algorithms for the Flux Split Euler Equations. NASA TM-2829.

[37] **Branth, A.,** October 1980. Multilevel Adaptive Computations in Fluid Dynamics, AIAA Journal, Vol. 18, No.10, pp. 1165-1172.

[38] **Beam, R. and Warming, R. F.,** September 1976. An Implicit Finite Difference Algorithm for Hyperbolic Systems in Conservation Law Form, Journal of Computational Physics, Vol. 22, pp.87-110.

[39] **Rumsey, L. C. and Biedron, R. T.,** June 1998. CFL3D User's Manual, Version 5.0, NASA/TM-1998-208444, NASA Langley Research Center, Hampton, VA, USA.

[40] **Hirsh, C.,** 1990. Numerical Computation of Internal and External Flows, Vol. 2, pp. 344-402.

[41] **Fletcher, C. A. J.,** March 1991. Computational Techniques for Fluid Dynamics, Second Edition, Vol. 2, pp. 40-42.

[42] **Mason, W. H.,** January 1982. Wing Canard Aerodynamics at Transonic Speeds Fundamental Considerations On Minimum Drag Spanloads, AIAA Journal 82-0097.

[43] **Baysal, O. and Yen, G. W.,** September 1997. Effects of Efficiency Techniques on Accuracy of Dynamics-Overlapped Grids for Unsteady Flows, Journal of Fluid Engineering, Vol. 119, pp. 577-583.

[44] **Yen, G. W.,** May 1994. Unsteady Flow Simulations About Moving Boundary Configurations Using Dynamic Domain Decomposition Techniques, Ph. D. Dissertation, Mechanical Engineering Department, ODU.

[45] **Ferziger, J. H and Peric, M.,** 1999. Computational Methods for Fluid Dynamics, Second Edition.

[46] **AMTEC Engineering Inc.,** 1998. TECPLOT Reference and User's Manual, Version 7.5, Bellevue, WA, USA.

BIOGRAPHY

First Lieutenant İ. Cenker Aslan was born on June 20, 1974, in Civril, Denizli, Turkey, where he received his elementary and secondary school education. He was assigned to Maltepe Military High School, Izmir, Turkey, and graduated in 1992. Afterwards, he received a Bachelor of Science degree in aeronautical engineering from the Turkish Air Force Academy, Istanbul, Turkey, on August 30, 1996, and he graduated from the Air Force Academy as a Second Lieutenant on that same date.

He received his initial pilot training at Second Air Force Base and Flight Training Center, Izmir, Turkey, from August 1996 through March 1998. After completing F-4E combat aircrew training at Third Air Force Base, Konya, Turkey, with the 1st degree, he was assigned to the 111th Squadron, 1st Air Force Base, Eskisehir, in October 1998 as a fighter pilot. He was promoted to First Lieutenant on August 30, 1999. While working in this squadron, he was assigned to a special Masters of Science program that was created by Istanbul Technical University, Istanbul, Turkey, and Old Dominion University, Norfolk, VA, USA.

First Lieutenant Aslan is a command pilot with 750 flying hours, including more than 500 hours as a wingman with F-4E and a modernized version of F-4E, the F-4E/2020 aircraft.